

Chen Shukar

06060231

ex 1

93 HJ

$$\textcircled{1} \quad \lambda = 620 \text{ nm} \quad V = \frac{1}{\lambda} = 1.6 \times 10^3 \text{ nm}^{-1} \times \frac{1 \text{ nm}}{1 \times 10^7 \text{ cm}} = 1.6 \times 10^4 \text{ cm}^{-1}$$

$$E = h\nu = \frac{ch}{\lambda} \rightarrow E = \frac{3 \times 10^8 \text{ m/sec} \times 6.63 \times 10^{-34} \text{ J.sec}}{6.2 \times 10^7 \text{ m}} = 3.2 \times 10^{19} \text{ J/photon}$$

$$E \cdot N_A = 3.2 \times 10^{19} \text{ J} \times 6.022 \times 10^{23} \text{ mol}^{-1} = 103.2 \text{ KJ/mol} = 2 \text{ eV} = 46.12 \text{ Kcal/mol}$$

$$\textcircled{2} \quad f = \left( \frac{8\pi \text{ MeV}}{3h e^2} \right) \frac{1}{M_i} = 10^5 \frac{1}{M_i} \text{ eri}^2 \quad \text{Me} = 9.1 \times 10^{-31} \text{ kg}$$

$$f = \frac{8\pi \times 9.1 \times 10^{-31} \text{ kg} \times 4.84 \times 10^{14} \text{ 1/sec}}{3 \times 6.63 \times 10^{-34} \text{ J.sec} \times (1.6 \times 10^{-19})^2 \times (\text{eri})^2} = \frac{4.84 \times 10^{14} \text{ 1/sec}}{r_i^2} \quad r_i = 0.4 \text{ nm} = 4 \times 10^{-10} \text{ m}$$
$$= 2.16 \times 10^{56} \frac{1}{\text{m}^2 \text{ sec}^2} \times [1.6 \times 10^{-19} \cdot (4 \times 10^{-10} \text{ m})]^2 = 0.88 \text{ 1/sec}$$

\textcircled{3}: The frequency of the oscillator is depending on the mass of the particle in the following way:  $\omega = \sqrt{\frac{k}{m}}$  therefore we can say that the frequency is proportional to  $\frac{1}{\sqrt{m}}$  - since  $E_{\text{vibration}} = \hbar\omega(V + \frac{1}{2})$  we can also say that  $E_v \propto \frac{1}{\sqrt{m}}$ .

It means that for a heavy particle we will get smaller gaps ( $\Delta E$ ) and for lighter particles larger gaps.

heavy atoms

light atoms

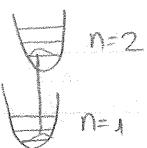
what about the shape of the potentials?

what will happen with isotopes?

④ a. Born-Oppenheimer suggests that we can treat the electronic wave function and the nuclei wave function separately since the  $e^-$  moves much faster than the nuclei - that can be therefore treated as stationary in that stage. The Frank-Condon principle uses the different time scale of this movement (electron vs nuclei) to explain why rigid system's absorption is higher than flexible ones.

The FC principle state that the absorption of a photon by an  $e^-$  is faster than the time it takes the nuclei to rearrange itself in the new vibronic band. The movement of the nuclei comes later and relaxes the system to a preferred vibronic state.

If the molecule is rigid- it means that the excited state geometry will be similar to that of the ground state:

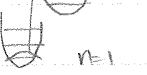


If the molecule is flexible, the

nuclei are free to adjust in a different manner

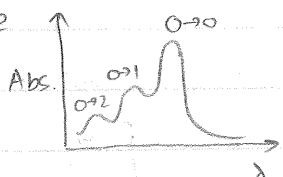
such as:

the result of these changes will be splitting

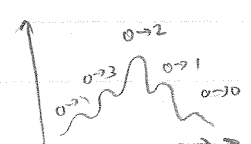


in the overlap of the vibronic levels ( $n=1 \& n=2,3$ )

In a rigid system we would expect to get a high probability transfer to  $0 \rightarrow 0$  and lower to higher vibronic levels and the UV-VIS will look like

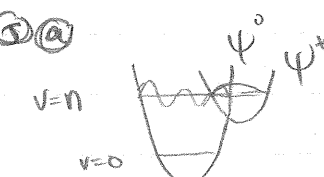
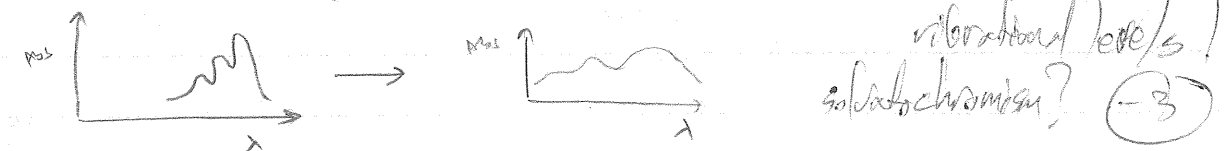


While in the flexible system we will get a higher probability transfer to different vibronic level which has a better overlap with the ground state which will yield a UV-VIS spectra such as:

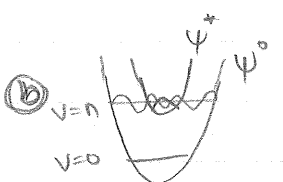


④b In solution, the solvent molecules interact with the material - first the  $e^-$  absorber a photon - in a vertical transition, and then there will be rearrangement of the solvent molecules around the excited molecule and will stabilize it.

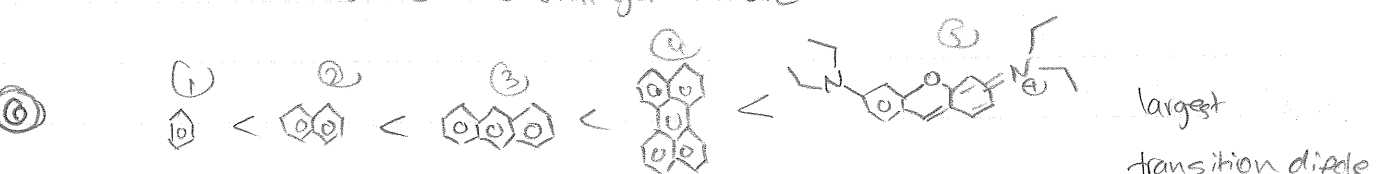
This effect leads to a reduction in the systems energy in general and will cause loss of resolution in the resulting UV-Vis spectra due to the interaction with solvent molecules. - of the following vibrational level(s) solvatochromism? (-3)



When there is a good overlap between some vibronic state in the ground state and the excited state we will expect an efficient radiationless transition.



When there is a poor positive overlap between the excited state and the N vibrionic level of the ground state we will get an inefficient radiationless transition.



As the conjugated  $\pi$  system is growing so does the transient-dipole, and S will have the largest transition dipole since it has  $\delta^+$  donor and  $\delta^-$  acceptor in 2 different sides of the molecule.

## Ex. 2

### (2) Polarizability

In general, the ability of a molecule to absorb light depends on the molecule's polarizability. The polarizability is determined by the number of delocalized electrons and the distance these electrons can travel in the molecule. The HOMO-LUMO gap defines the energy of the absorption - and  $\pi$  electrons are responsible for the absorption in the UV-vis range.

In addition, rigid systems like anthracene have a much better orbital overlap between the ground and excited state which allows an efficient vertical absorption in such systems. Therefor the anthracene will have a higher extinction coefficient than dodecane. ✓

② Kasha's rule claims that radiative processes will occur from the lowest excited state of a given multiplicity, no matter which higher level was excited.

This transition from the lowest excited state happens because of radiationless transitions that are taking place much faster than the fluorescence we obtain.

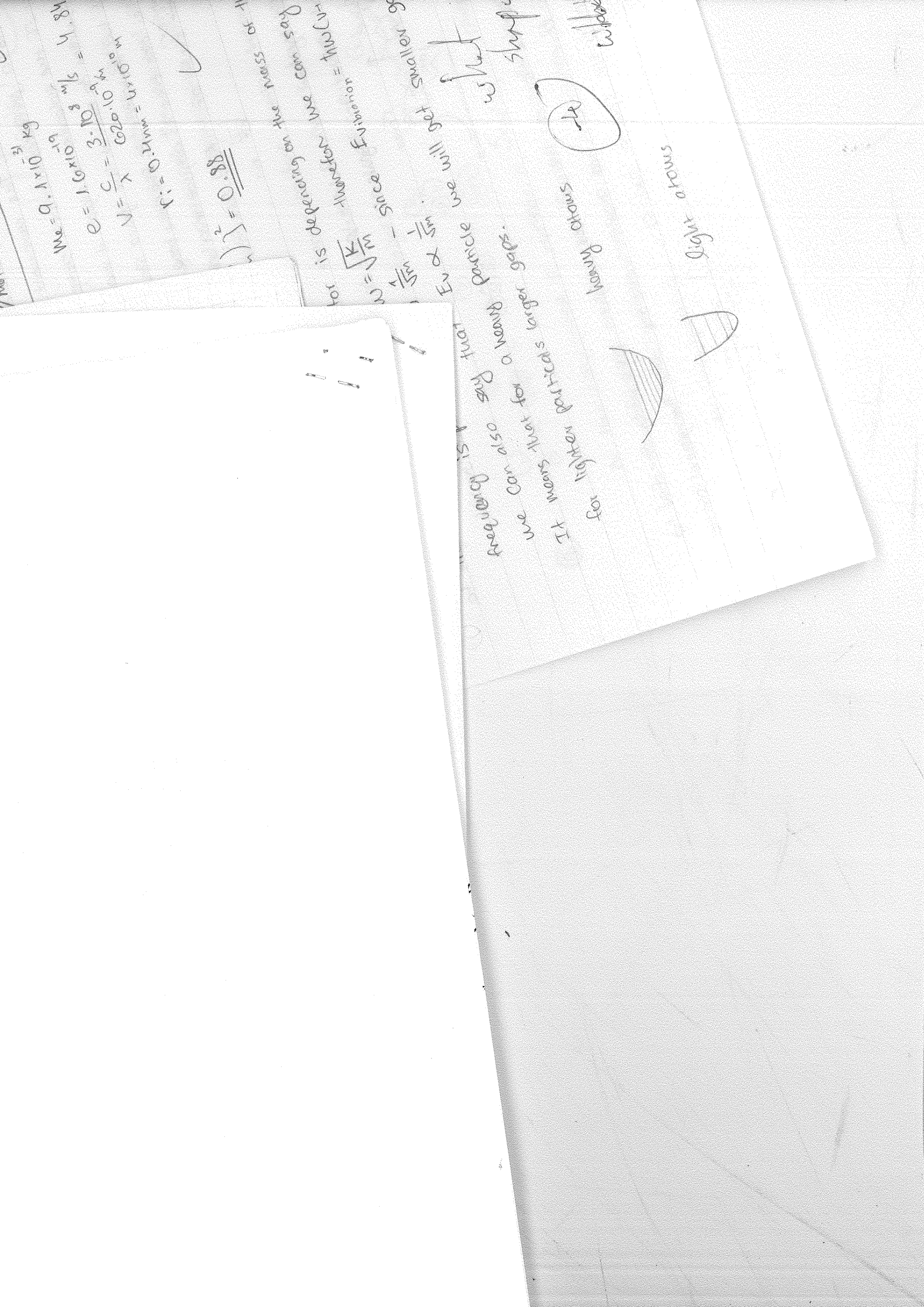
The overlap between the vibrational levels of higher excited states is good and their vibrations occur in a timescale of picoseconds,

while the fluorescence happens on a nanoseconds timescale. ✓

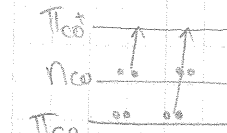
$\Phi$  is the measure of the efficiency of radiative transition, and it will be higher in molecule C, since D has more vibrational levels (more groups that can contribute to vibrations) and will create more non-radiative transitions that will reduce the efficiency of the radiative transition.

③ According to the Hund's Rule Revisited the singlet to triplet transition has first an increase in energy due to symmetry changes of the function and then a decrease of energy due to lower kinetic energy and smaller orbital size -

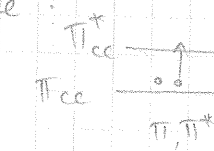
which leads to a higher attraction between the electron to the nucleus → and decreases the total energy of the triplet state. Mulliken said that as we go higher into calculations we tend to lose the grasp of the chemical guiding concept - we would like to have a level of understanding that will be justified →



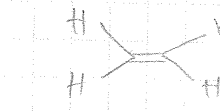
#### (4) formaldehyde:



$\pi \rightarrow \pi^*$

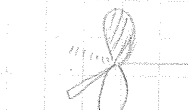


H) ethylene:



In the case of formaldehyde, the transition from  $\pi \rightarrow \pi^*$  will look

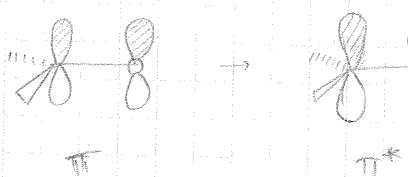
as follows:



angular momentum change  
spin momentum change

The overlap integral is small since the orbitals are perpendicular to one another, that will lead to a small  $J_{\pi\pi^*} \langle \pi | \pi^* \rangle$

whereas in ethylene we will get the  $\pi \rightarrow \pi^*$  transition that will appear as:



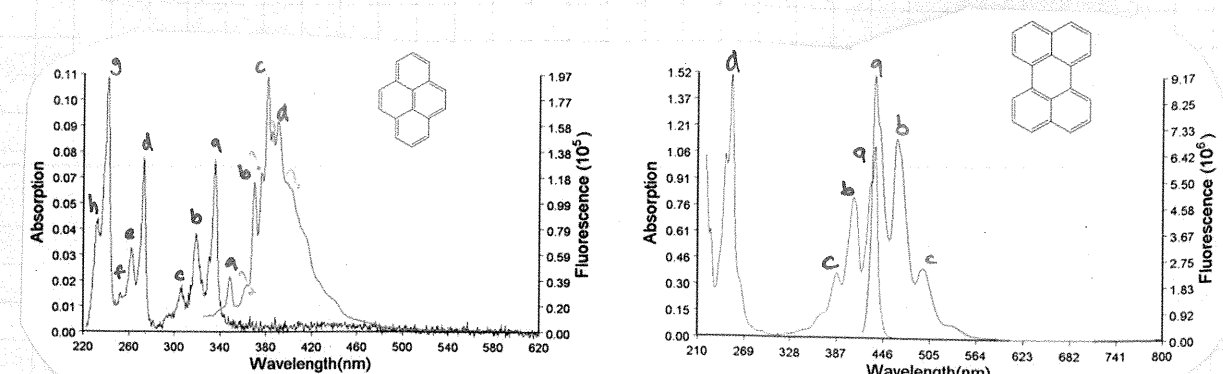
and the overlap integral is large,

$J_{\pi\pi^*} \langle \pi | \pi^* \rangle$  is large.

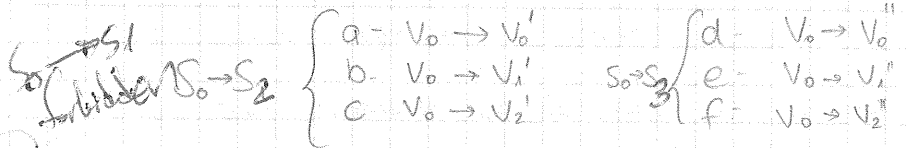
The splitting of  $S_1$  and  $T_1$  in the case of  $\pi | \pi^*$  will be smaller than in the case of  $\pi, \pi^*$  since there will be less electron repulsion, that means  $\Delta E^{\text{ST}}$  is small in formaldehyde and allows efficient intersystem crossing while in the case of ethylene the large gap ( $\Delta E^{\text{ST}}$ ) will inhibit it.

$\dots \rightarrow \text{red}$

in QM terms but will still be understandable in means of the chemical concept.

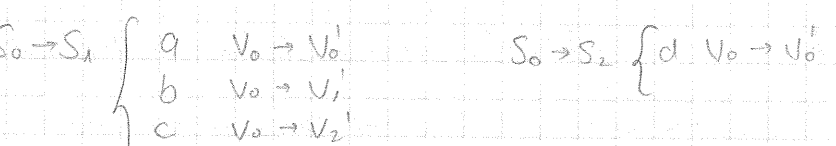


a) in E a-h are the absorption peaks:



a-d are emission peaks  $S_2 \rightarrow S_0$  from different vibronic states, the resolution of these transitions is not very clear so it is difficult to name them.

a-d are the absorption peaks



a-c are emission peaks



b) Stokes shift is the difference in wavelength between  $\lambda_{\text{max}}^{\text{absorption}}$  and the  $\lambda_{\text{max}}^{\text{emission}}$ .

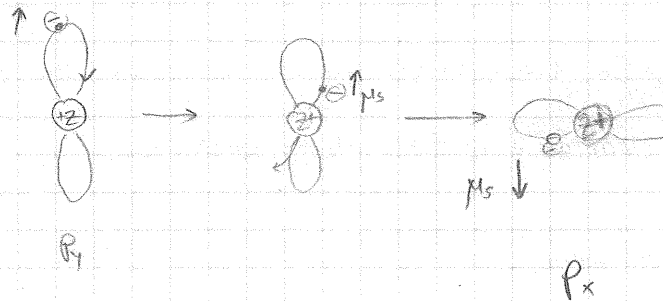
By looking on the spectra of  $\text{CF}_3$  we can say that F is a more rigid system than E since it has a smaller Stokes shift. When the Stokes shift

in geometry- there wasn't major change and re-arrangement of the nuclei

after the excitation of the electrons. That means that F has a larger similarity between its ground & excited states than E has.

c) We can see that in system E the emission spectra has a not very clear vibronic peaks and it does not resemble the absorption spectra, while in F - the emission is like a mirror image of the abs. and has very defined vibronic bands - which is very common in rigid systems since the excited and ground state are similar they have similar transitions.

- ⑥ spin orbit coupling is the simultaneous change of the spin moment and the orbit moment while keeping the total angular momentum fixed.



The electron orbit can be looked at as a harmonic oscillator, where at the far ends from the nucleus the velocity is low and closer to the nucleus the velocity is maximal. Since the electron is charged, it generates magnetic field-

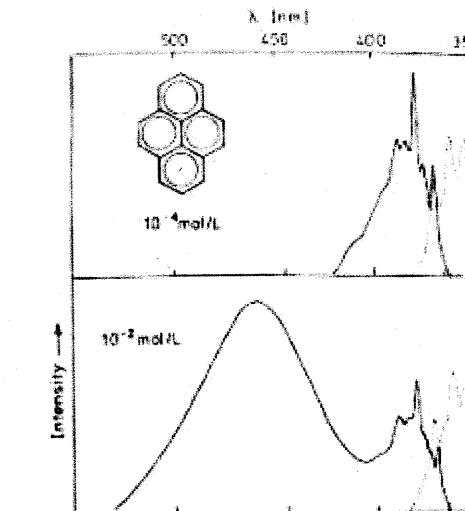
which also will be maximal when the velocity is maximal - close to the nucleus. The magnetic torque acts on the electron's magnetic spin moment to induce a flip and simultaneously the orbital angular momentum changes as well - conservation of the total angular momentum of the system.

The heavy atom effect is connected to the spin orbit coupling by the fact that a heavy atom has a higher  $Z+$ , which in turn effects and increases the velocity  $\rightarrow$  creates larger magnetic field and torque and enhance the probability for the flip and coupling.

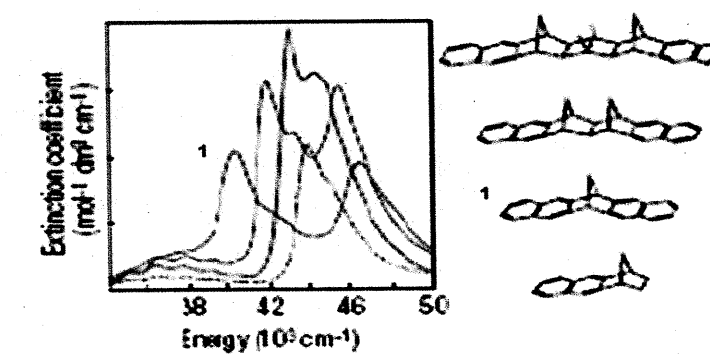
# Molecular Photonics

## Exercise 3

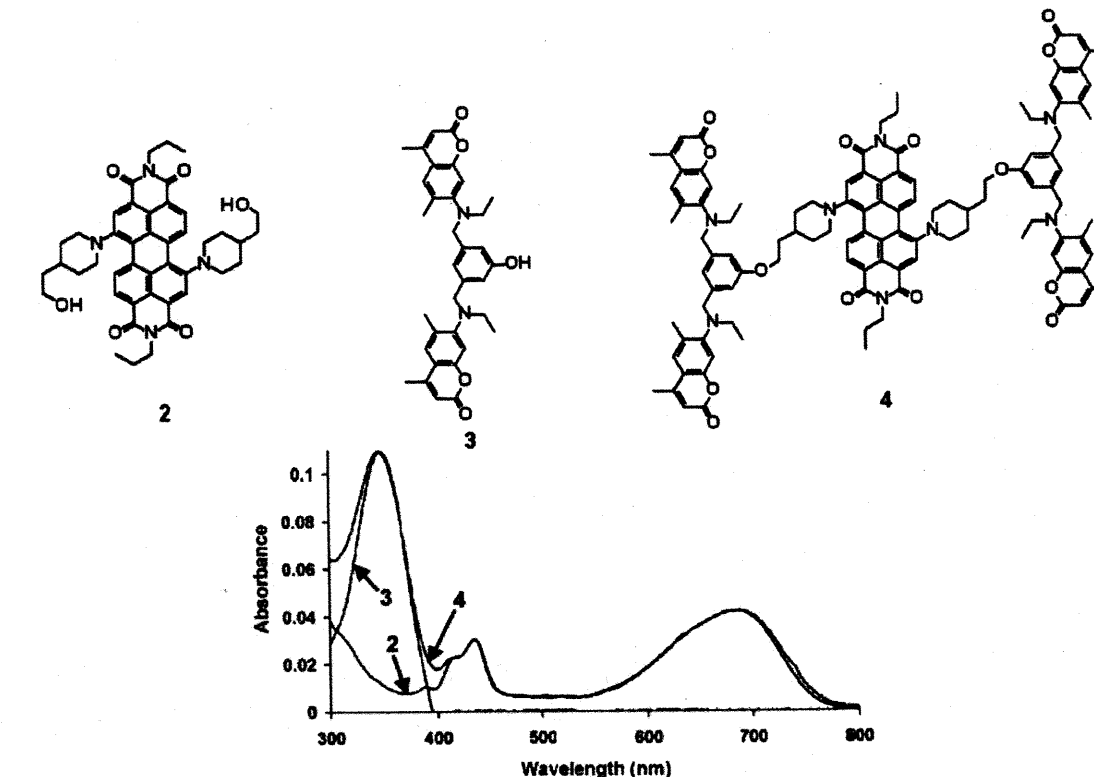
1. What is an excimer?
  - a. Draw a MO scheme that represent excimer formation.
  - b. Draw schematically the potential energy curves that represent excimer formation and the differences between monomer and excimer fluorescence. Explain the expected differences in the shape and wavelength.
2. In the two UV-vis/Fluorescences spectra of pyrene below there are major differences.
  - a. Suggest an explanation (notice the concentrations).
  - b. What changes can one expect in the fluorescence spectra at higher concentrations? Suggest what will happen to the fluorescence spectrum of pyrene in crystal form.



- c. Suggest one biochemical application for pyrene excimers.
3. Draw the four situations of exciton energy level splitting using Kasha's theory. (Kasha et al. *Pure Appl. Chem.* 1965, 11, 371-392.)
  - a. Explain shortly the reason for the energy stabilization and allowedness of each level.
  - b. Explain using the answer to question 3a the spectrum below what can be said regarding the relative position in space of the naphthalenic moieties of dimer 1. (monomer's trace is in black),



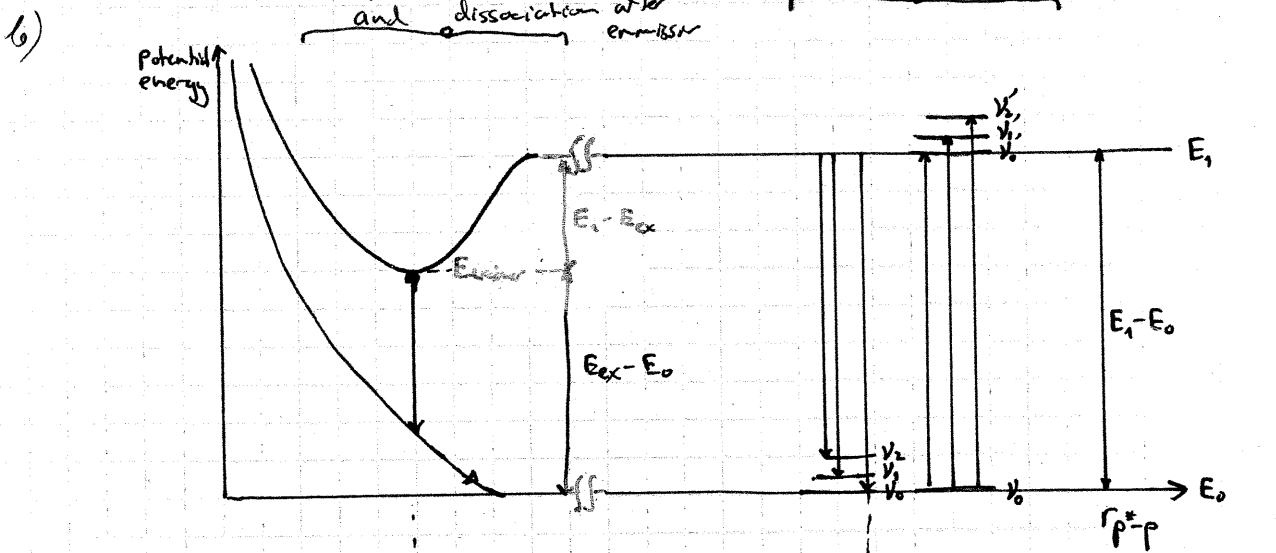
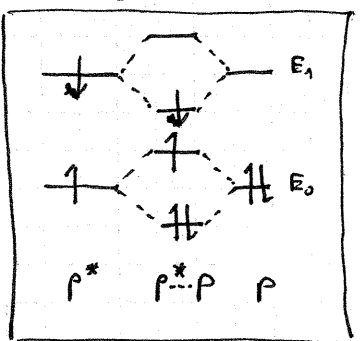
4. What are the three mechanisms for energy transfer between two molecules?
- Draw schemes and explain each mechanism.
  - Which one is the most common?
  - In what specific case the answer for question 4b is not the dominating mechanism? Explain.
5. By what means one can detect energy transfer between molecules?
- Give an example for a system like this. Draw schematically the molecular system and the spectra of the different components.
6. Compound **2** is a perylene diimide derivative. Compound **3** is a coumarine derivative. Compound **4** is the combination of both. The figure below shows the UV-vis spectra of all the three compounds. The spectrum of **4** is the sum of the spectra of **2** and **3**. (Fréchet et al. *J. Am. Chem. Soc.* 2002, 124, 11848-11849)
- Describe shortly what will be observed in the emission spectra when compound **4** will be excited at 380 nm and 750 nm.



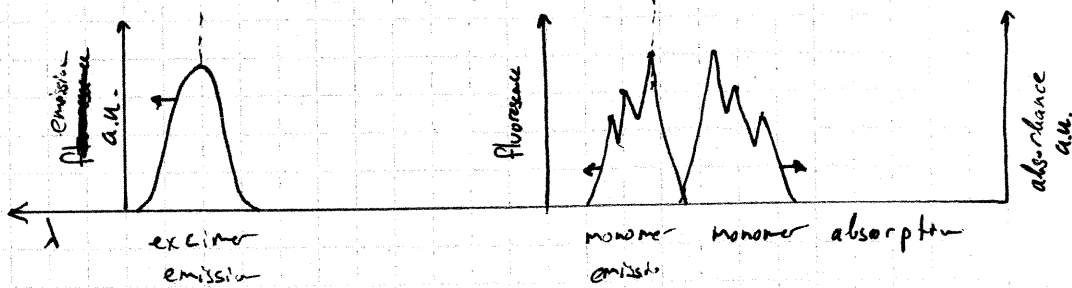
- Draw a schematic energy level diagram that describes the photophysical processes that occur in this system.
- What is the energy transfer efficiency that was found for the system by Fréchet and coworkers? What will happen to it if the distance between **2** and **3** will increase? Suggest a general way to check that. What dependency on the distance will be found?

1) An excimer is a collision (or an excited state dimer) where the original excitation of one of the monomers is shared with an identical monomer which is at its ground state. The excimer is also characterized by dissociation at its ground state.

a) Two of the three electrons in the ground state of  $P$  and  $P^*$  are stabilized and the remaining one is destabilized. The electron in the first excited state of  $P^*$  is stabilized so in total 3  $e^-$  are stabilized and one is destabilized.



the spectra will have these general features as follows :



the excimer has a lower energy due to net stabilization and therefore its emission is red-shifted. Due to a much larger density of vibrational states in the excimer the excimer emission spectra is smoothed.

M&amp;I

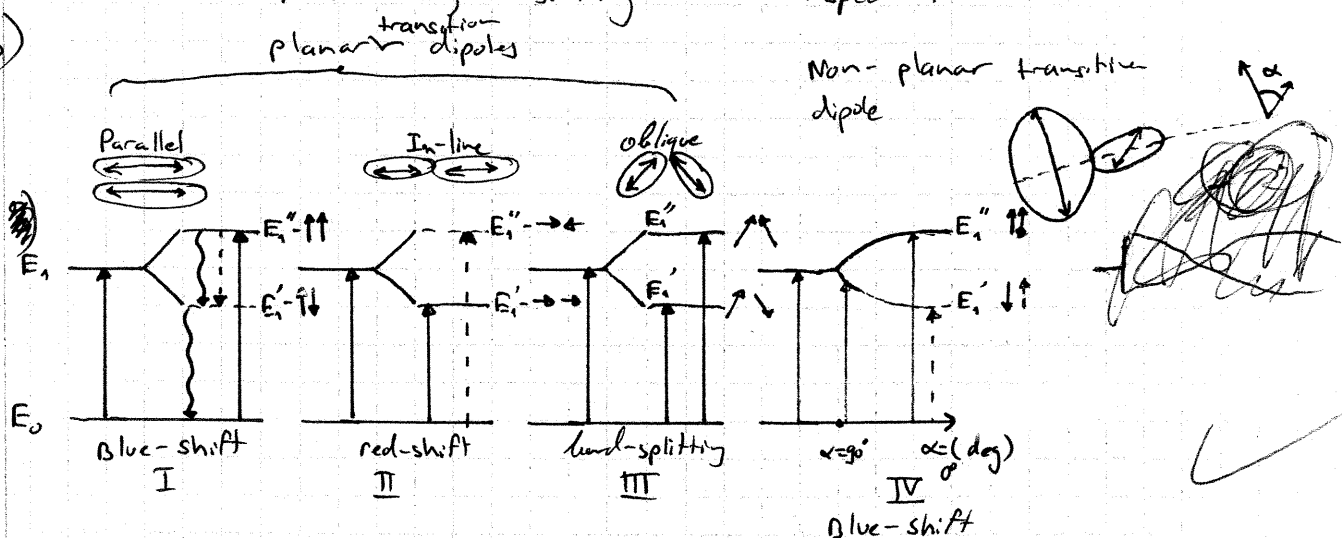
In addition, the short lifetime of the dissociated excimer also prevents the clear resolution of vibrational bands. The large density of vibrational states is due to the large number of possible mixing of the individual vibrational states as well as the large number of forming it as a result of the distance.

(3)

Molecular photonics of organic compounds - Ex3 - Roi Levi - 034956813 - 30/12/8 - chem. - M&I.

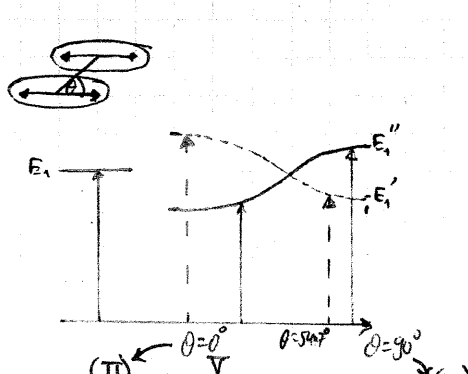
- 2) a) It would seem that on some of the excited pyrene molecules form excimers. This can be inferred from the appearance of new smooth fluorescent emission at a higher wavelength than the monomer emission, which in turn decreases in intensity, due to the increase in the concentration.
- b) One can expect that at even higher concentrations the monomer fluorescent spectra will vanish almost entirely and the excimer emission will increase. I assume that in the crystal the monomer emission will vanish entirely.
- c) The study of protein conformational changes could be studied *in-vivo* by functionalizing the protein at select locations with pyrene and then one can infer the distance between them by observing the emission spectra.

3)



I and two can be thought as the extreme cases of IV

co-planar -



\*the LHS of each diagram are the monomer levels and the RHS are the dimer levels

(4) Molecular photonics of organic compounds - Ex 3 - Roi Levi - 0349356813 - 30/12/8 - chem  
M&I.

- a) I. In  $E_1'$  the dipoles are out of phase and this corresponds to an electrostatic interaction that lowers the energy of  $E_1'$  compared to  $E_1$ . The opposite is true for  $E_1''$ . The transition dipole is given by the vector sum of each  $\vec{d}$  <sup>transition</sup> and since this sum is zero for  $E_1'$  it is forbidden. It should be noted that the ~~ex~~ fluorescence will be quenched due to fast Non-radiationless decay (IC) to  $E_1'$  and since the radiative transition is forbidden we will either get IC or inter system crossing (ISC) to a triplet state which then may give phosphorescence. the absorption spectra will be therefore blue shifted.
- II.  $E_1'$  is lower in energy since the in-phase dipole ~~arrangement~~ arrangement is lowered by the electro-static (ES) interaction.  $E_1''$  is forbidden since the vector sum is zero. the absorption and probably the emission spectra will be red-shifted.
- III. Again, in  $E_1''$  the ~~interaction~~ interaction lowers  $E_1''$  in energy and the opposite is true for  $E_1'$ . However in this case the vector sum is equal and non zero in both cases so both of them are allowed. We will get splitting of the spectra.
- IV. for  $\alpha = 90^\circ$  there is no difference between the two and as  $\alpha \rightarrow 0^\circ$  we go to I. ✓

- b) It can be seen that the extinction coefficient for each peak in  $\text{I}$  is roughly the same and in addition the splitting is quite large which rules out  $\text{IV}$  and leaves us only with  $\text{III}$  - oblique dipoles one to the other. This is strengthened by the two other spectra where as the dipoles are separated further apart the electrostatic interaction weakens which results in a smaller splitting between  $E_1'$  and  $E_1''$  (smaller  $H_{LR}$ ). ✓

b) I requires:  $QY_0 \approx 1$ , high conc. of A, high ex. coeff. of A and a good high value for the spectral overlap integral (overlap between D's emission and A's absorption).

III requires: physical contact between A, & O<sup>+</sup> or collision (exponential dependence on distance) in order to get orbital overlaps, high J. It is a short range mechanism and is also negatively affected by diffusion.

II requires: sufficiently close ( $\propto r^{-6}$ ), large J, relative dipole orientation and dielectric constant. This is a long range mechanism.

Survey: It can be seen that II should be the most common as its requirements are the least stringent! It is activated ~~over~~ at much larger distances than I, III; ~~and~~ does not ~~contain~~ physical transfer of e<sup>-</sup>'s or photons.

+1  
for best answer

c) FRET may be inhibited when the excited state in question is a triplet: the triplet dipole has a low dipole strength thus reducing the FRET efficiency while the triplet excited species has a longer lifetime thus increasing the Dexter exchange mechanism efficiency, by increasing the probability for a collision.



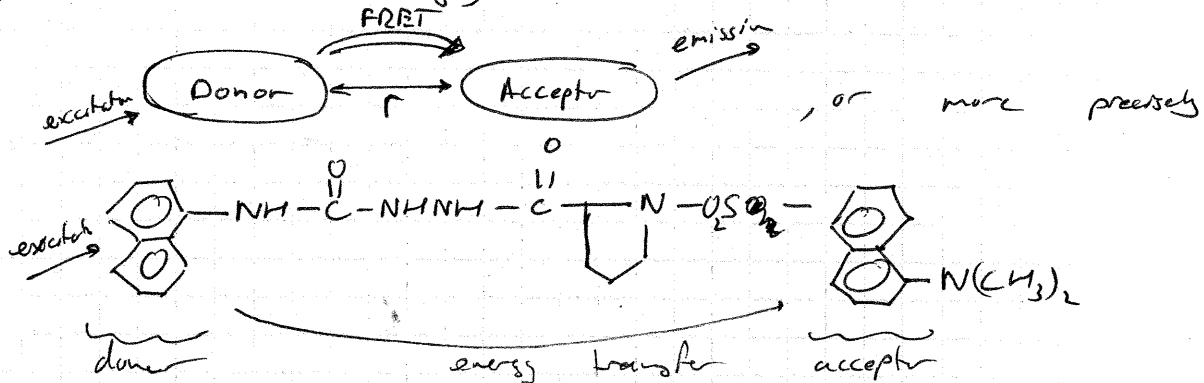
5) If these molecules act as a donor and acceptor

species then the energy transfer can be inferred if,

- the acceptor emission is enhanced when the donor is excited while the donor emission is quenched

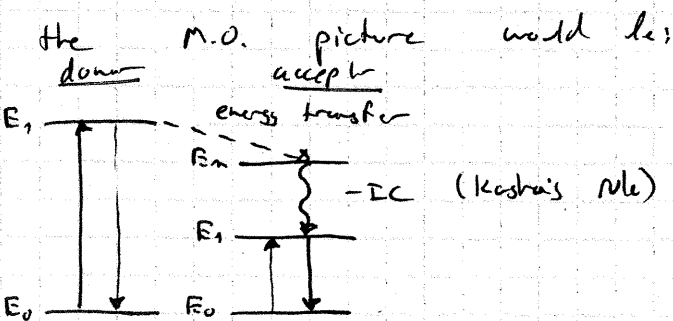
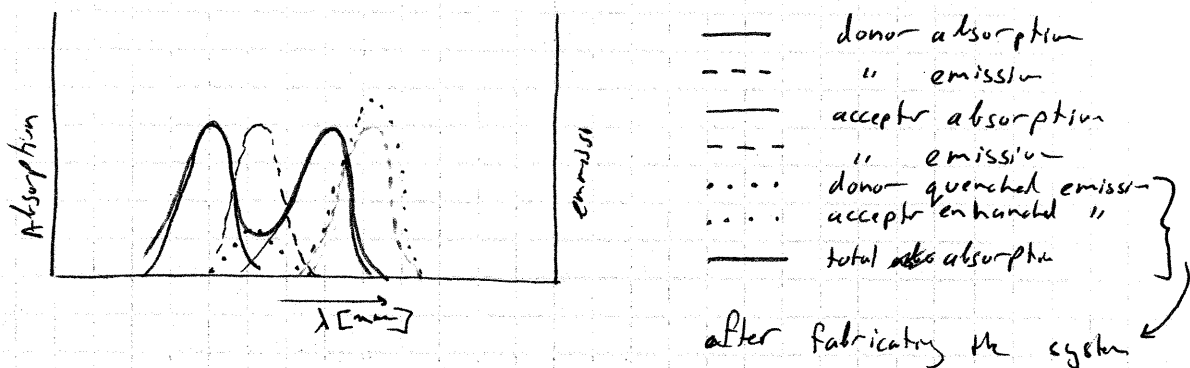
- the combined absorption of the donor and acceptor system remains roughly the same.

a)

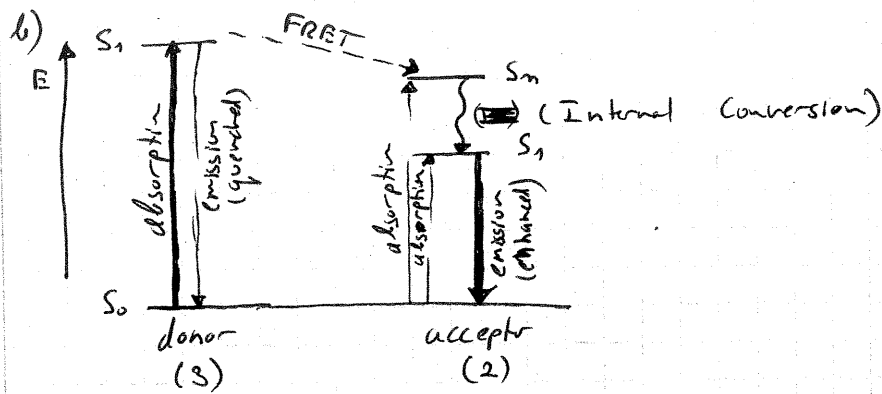


, or more precisely

where the spectra would look like this:



6) a) When compound 4 will be excited at 380 nm we will only see emission from the acceptor (compound 2). However, when we excite at 380 we will see a quenching of the emission of the donor (compound 3) and enhancement of the emission of the acceptor due to its ability to absorb at 380 nm and the energy transfer from the donor.



only the RMS (without the FRET) will occur when exciting at 780 nm and the whole scheme will take place when exciting at 380 nm.

c) Fréchet et al. found an efficiency of 99%. If the distance between 2 and 3 will grow the enhancement effect should weaken. A general way to check this should be by repeatedly elongating the donor-acceptor connection. Under the assumption that the energy transfer mechanism is FRET the dependence on the distance should be: FRET efficiency  $\propto R^{-6}$  where  $R$  is the distance between the donor and the acceptor.



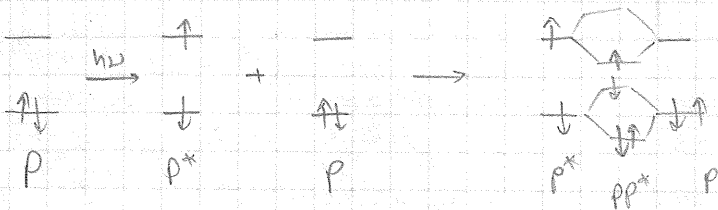
## Molecular Photonics - EX 3

Chen Shuhar  
09/09/2023 11

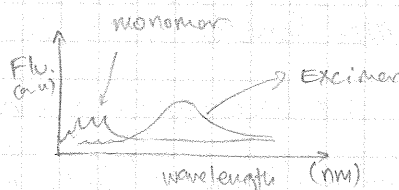
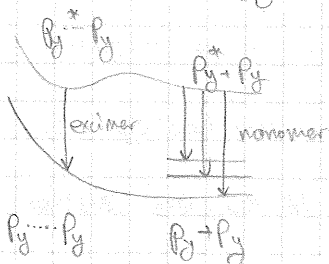
① An excimer is a case where two molecules of the same kind are dissociated

in the ground state, but have a joint excited state that the two exit from.

a)



b) Potential energy:



The excimer will be red shifted - will have lower energy than the monomer

due to stabilization occurring in this state. Moreover, the excimer will have a higher density of vibrational states that will result in a broadened and smoothed spectra.

② a) In the concentrated solution the probability to form excimers is higher,

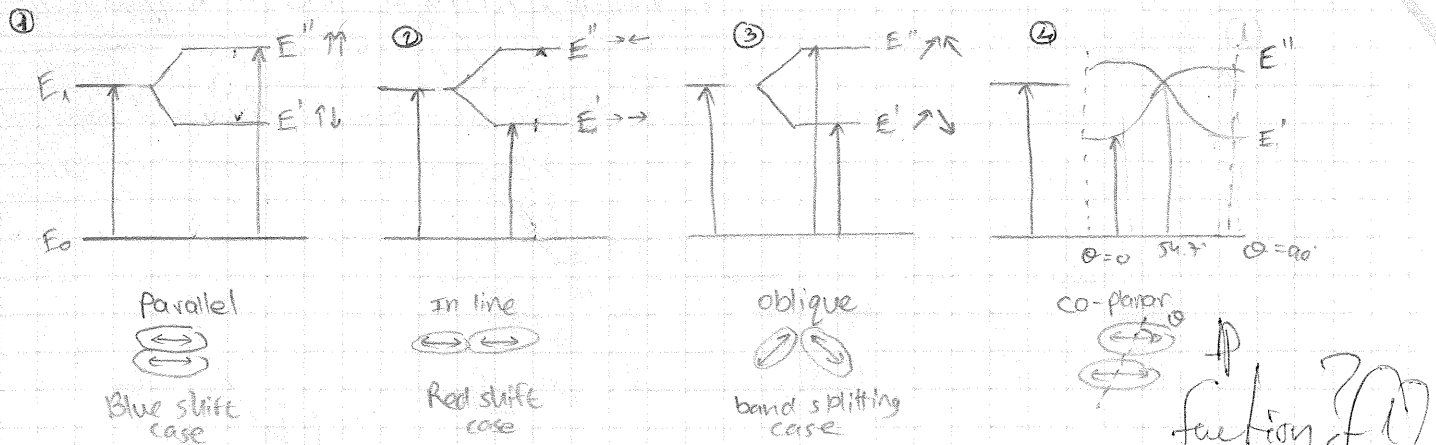
and as a result we will get a monomer emission spectrum - top one, and an excimer pattern.

b) At higher concentration we will get more of the excimer pattern in the flu. spectra and less of the monomer. In the crystallized pyrene I would expect to get only excimeric pattern - all the material would be arranged as dimers.

c) Is it possible to use it as a "distance marker" meaning - the excimer would not form unless the two molecules creating it will be in close proximity to one another. In the case one needs to prove that two biological sites (2 proteins interaction) are coming together - it can be

proven by attaching to each protein/site one molecule and detect if indeed there is close proximity - excimeric pattern, or not - monomer one.

(3) Kasha's model is based on the relative angle between two chromophores.



④ The left of each diagram represents the monomer levels and the right represents the excimer levels.

a) ① In the case of  $E'$ , we have opposite dipoles which can be seen as electrostatic interaction that lowers  $E'$  with respect to  $E_1$ , and makes  $E''$  higher in energy from the same reason. The total transition dipole will be given by the sum of the vectors, in the case of  $E'$  it will be zero and hence forbidden.

②  $E'$  here is also lower in this case due to electrostatic interaction.  $E''$  will be forbidden since the sum of the vectors is zero.

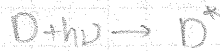
③ Some explanation about  $E'$  &  $E''$  lowers and higher in energy than  $E_1$ . Thanks to Electrostatics considerations. In this case the sum of the vectors is non-zero in both cases - they are allowed.

④ A range that corresponds to case ② with  $\theta = 0^\circ$  and to case ④ where  $\theta = 90^\circ$ .

⑤ It can be said that the position will be oblique since we have a band splitting and both bands are equally allowed.

⑥ The three energy transfer mechanisms are : a) radiative energy transfer, b) coulombic interaction energy transfer (Förster, FRET) c) exchange interaction energy transfer, (Dexter)

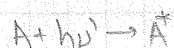
③ a) Radiative energy transfer:



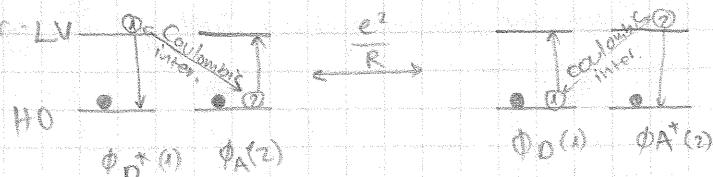
D absorbs light and emits in a longer wavelength,



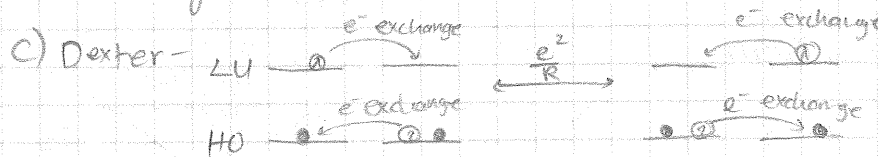
the emitted light is then absorbed by A.



b) Förster - LV



Upon absorption of light a transition dipole is formed and it is inducing a transition in a neighboring molecule via coulombic interactions. No direct orbital overlap is necessary.



Exchange mechanism, that needs a direct orbital overlap to transfer an electron from an excited molecule to its neighbor.

⑥ The Förster mechanism is the most common one.

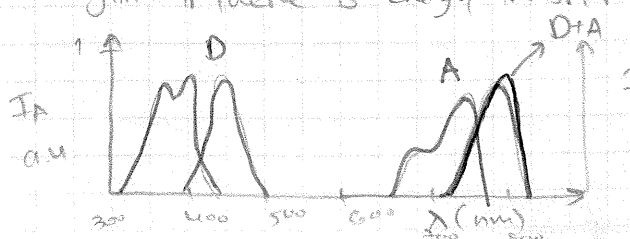
⑦ In the case of triplet state - the dipole moment is smaller and the Förster mechanism would be less effective. On the other hand triplet states are long-lived and can have a good orbital overlaps between the molecules and Dexter can take place. When there are collisions!

⑧ One can detect energy transfer by detecting the quenching of fluorescence

or the change in emission spectra. for example: if we have a system of 2 chromophores D & A, we can measure the UV-vis and fluorescence

of each of them separately in solution, and then mix them and measure

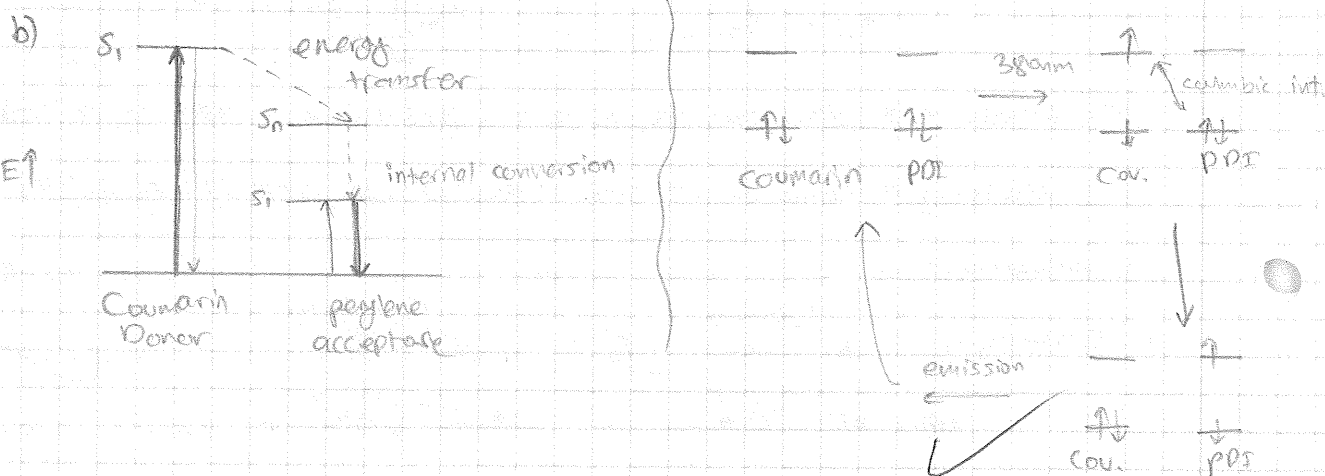
again - if there is energy transfer - we will get the following spectra:



IF  
a.u

The emission will be coming only from the A. which is lower in energy.

(6) a) When exciting at 350nm, we will get a typical fluorescence of the PDI derivative (2) because only the PDI absorbs in that wavelength. When exciting at 380nm - Coumarin will absorb more than the PDI - since the absorption efficiency is higher there, and most probably there will be energy transfer by FRET mechanism and we will get the emission spectra of PDI.



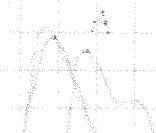
b) The donor emission was completely quenched due to the energy transfer and resulted in 99% energy transfer efficiency.

- When the distance between donor and acceptor will increase we would expect a decreased energy transfer, Förster efficiency goes as the inverse 6th order law due to the dipole-dipole coupling mechanism. A way to check it out is to connect a rigid linker between donor and acceptor, and measure a series of different linkers (in length) and see the dependency of  $F_0^6$  with the distance.

D - to - A

$$\frac{1}{1 + \left(\frac{R}{R_0}\right)^6}$$

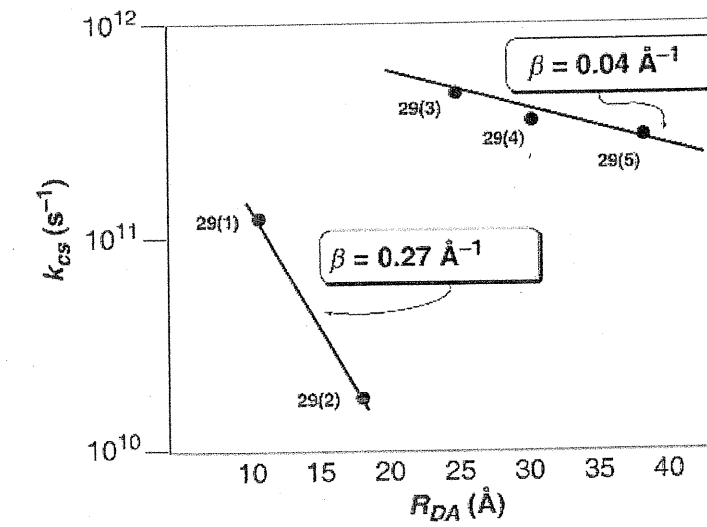
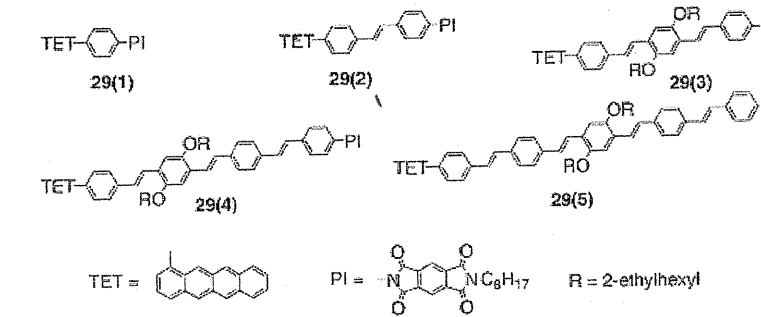
(2)



# Molecular Photonics

## Exercise 4

- a. Draw a diagram that illustrates the possible pathways for a charge separation process (electron and hole transfer).
- b. In vacuum there is a large dependence of  $k_{ET}$  over distance. What will happen when 1) the donor and acceptor are in a solvent, 2) there is a saturated hydrocarbon bridge between them?
- c. Explain what does  $\lambda$  represent and how it affects the rates of the process.
- d. Write down Marcus-Hush equation. What is  $V_{el}$  and how it is related to  $k_{ET}$  and to the distance between the donor the acceptor?
- e. What are the differences between a superbridge (superexchange regime) and a molecular wire? Explain and draw schemes if needed.
- f. The graph below describes the charge separation rate of molecules 29(1-5). Explain the observed rate trends in the graph.



$$\left(\frac{2}{3}\right)^2 = \underline{\underline{0.88}}$$

卷之三

depending on the noise  
we can say  
whether  $\text{Env}(N_{\text{vis}}) = \text{Env}(N_{\text{vis}})$   
since

As we will set smaller goals  
and we will feel better.

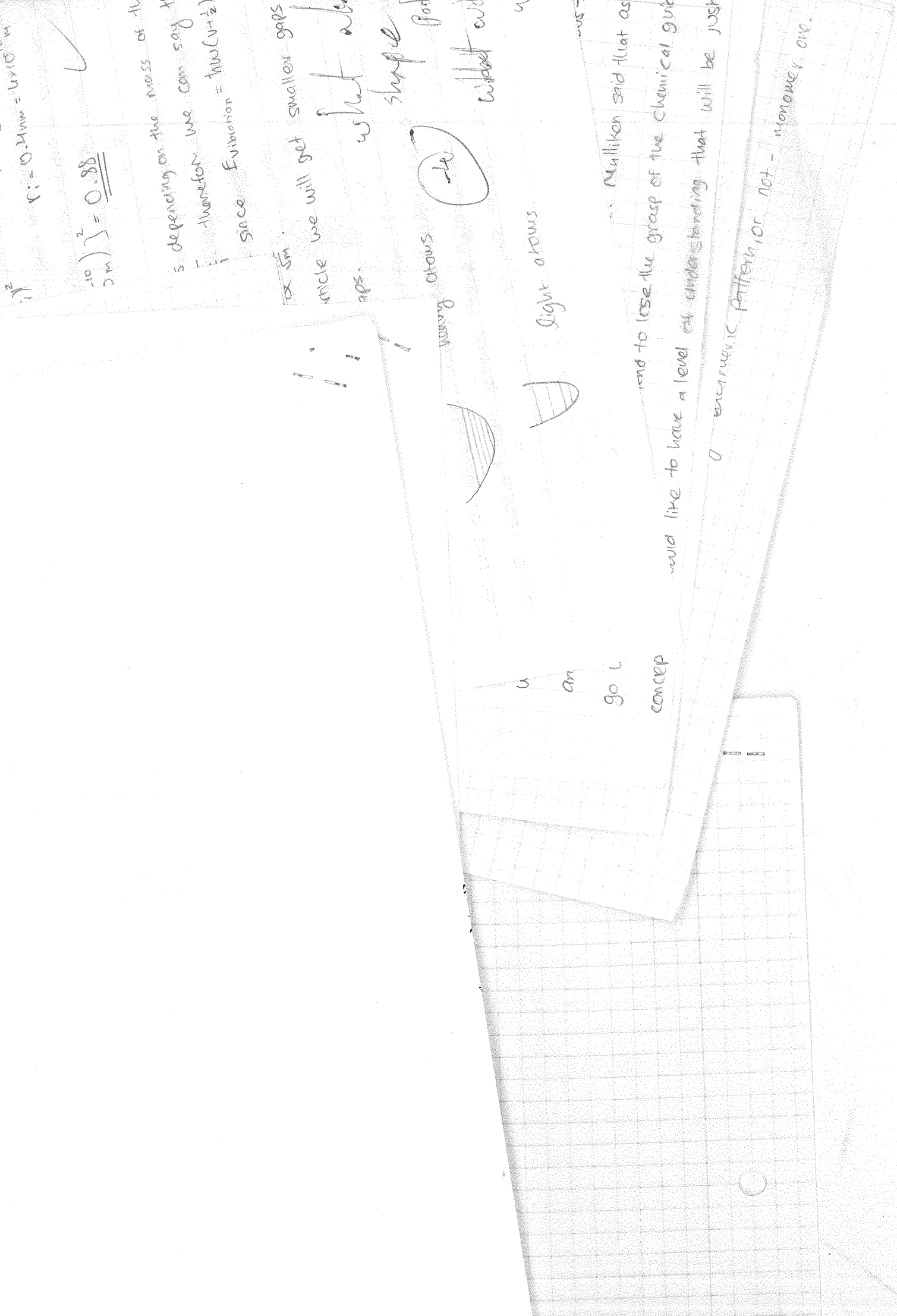
shape shows a lot of

What about  
right always

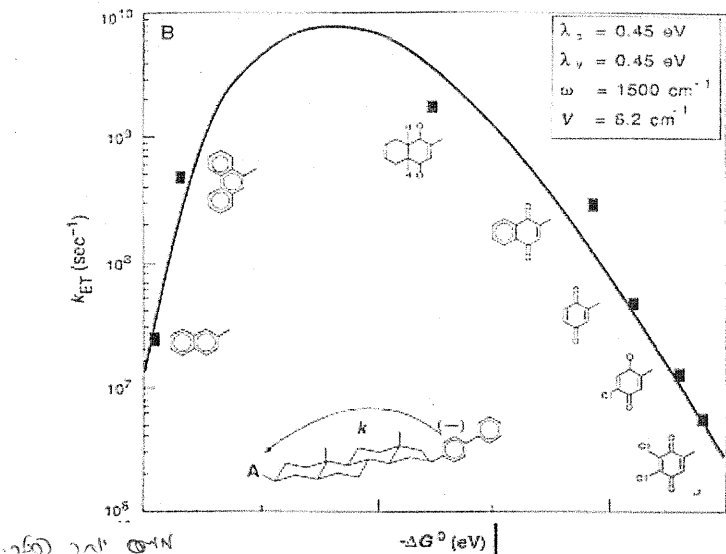
Millikan said that as we have grasp of the chemical quic

First of the Chemical guide  
understanding that will be just  
Pattern, or

or not - "monover" one.



- 2
4. The dependence of the electron transfer rate on the driving force is given below for a series of compounds in butyl ether (acceptor, A, is varied). Why is the maximum observed? How would the reorganization energy change if more polar solvent would be used?

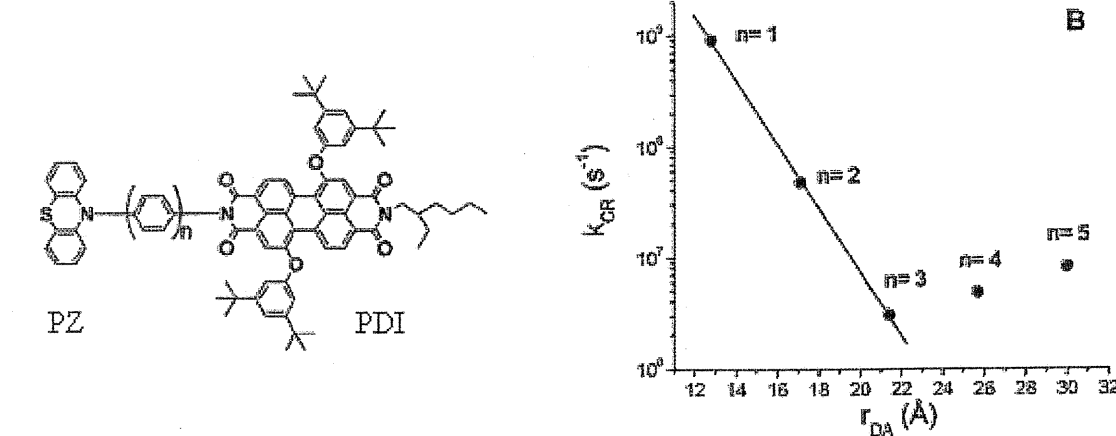


$-\Delta G_{CS} = \lambda$   
 driving force  
 $\propto 1/kT$   
 $-\Delta G_{CS} > \lambda$   
 inverted region is  
 $\propto 1/kT$   
 $-\Delta G_{CS} < \lambda$   
 driving force.

RIP

5. See below the structure of the donor-bridge-acceptor family of molecules. Photoinduced electron transfer (PET) takes place in all of these molecules.

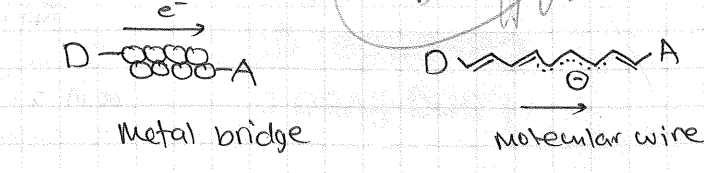
- b. Estimate, using Rehm-Weller equation the upper limit for the thermodynamic driving force of PET (Perylene diimide (PDI) 0-0 emission is at 565 nm, PDI one-electron reduction potential is -0.6 V, one electron oxidation potential > 2.0 V, one electron oxidation potential of phenothiazine (PZ) is 0.6 V)
- c. The rate of charge ( $k_{CR}$ ) recombination as a function of distance between donor and acceptor is given. Explain the observed behavior.



## Molecular photonics ex. 4

Qa. The 3 mechanisms for charge separation are:

\* Electrical conducting bridges:



transport of the electron through the conduction band of the bridge (metal), or through the resonance system (conducting polymer).

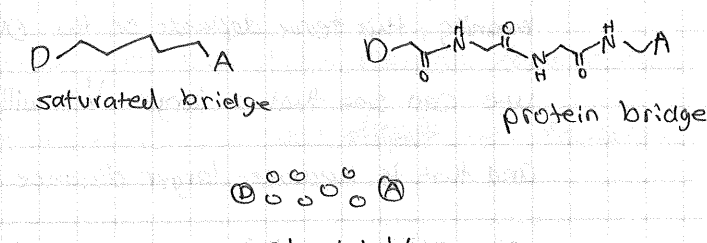
*This is 1)*

\* Charge-hopping bridges:

transport of the electron from donor to acceptor through bridge that is made of a few discrete units with similar redox potentials, each unit can get the electron for a short period of time and pass it to the next unit.

*answser for (3)*

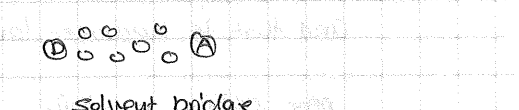
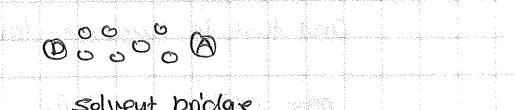
*see e-mail*



\* Electronically insulating bridges:

- Superexchange

The transition is from the donor wave function to the acceptor wave function.



b. In the case of a solvent and saturated hydrocarbons bridges the superexchange mechanism takes place, while in VACUUM ET occurs through the direct coupling between donor and acceptor - which is strongly dependent on the distance, large  $\beta$ . In the case of the solvent & the saturated bridge - they are "supplying" orbitals which the electrons can tunnel through.

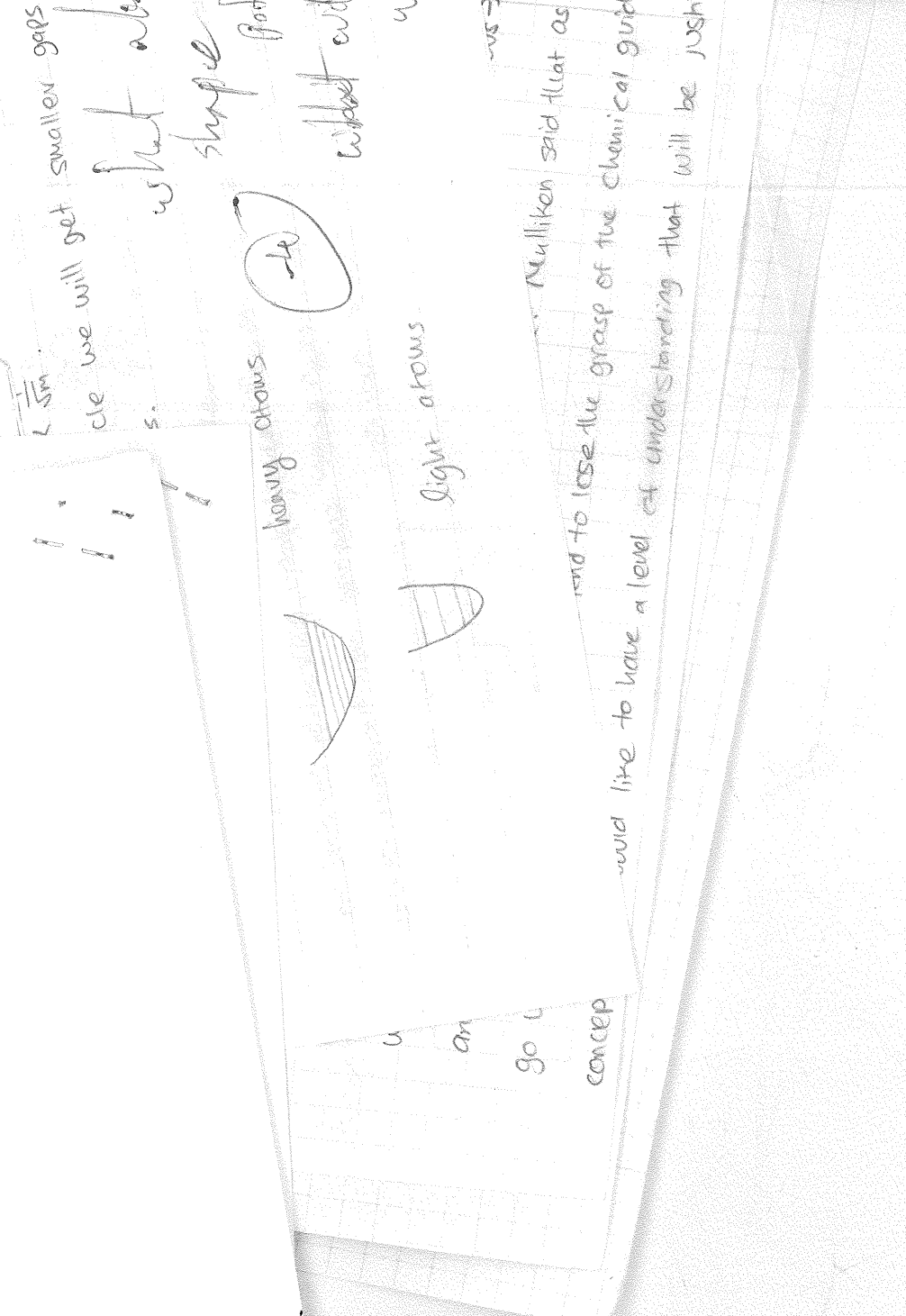
In a bridge the distances are smaller and the orbitals are relatively fixed compared to a solvent so I would assume the transition would be a bit more efficient.

Qa. Marcus used parabola geometry considerations to explain the basic principles of electron transfer and determine the process's rate.

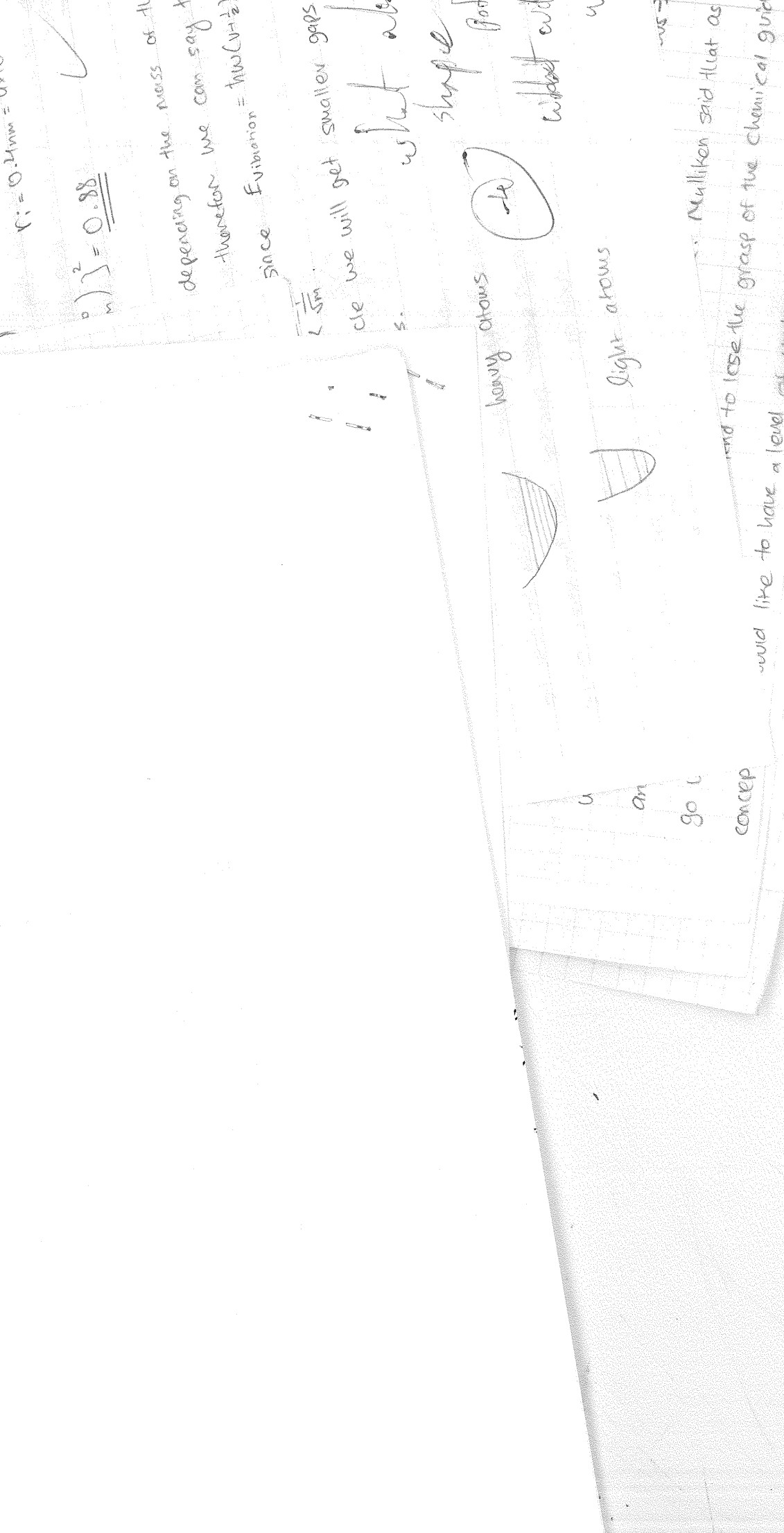
There are few factors that determine this rate:

- The distance between D and A (electron transfer is more efficient as this distance decreases)
- $\Delta G_{cs}$  the Gibbs energy - electron transfer is more efficient when  $|\Delta G_{cs}|$  is bigger.
- The reorganization energy,  $\lambda$  need for the molecular rearrangement of A, D and solvent molecules during an electron transfer.

The electron transfer rate will increase when  $\lambda$  is closer to the reactant's  $\Delta G_{cs}$ . When  $\lambda < \Delta G_{cs}$  we are in the inverted region - and the reaction will be slower.







- (3b) It seems that in 1&2 the mechanism of CS is the superexchange mechanism. It's easy to see that the longer the molecule the slower the reaction rate, which fits to the dependency on D to A distance in this mechanism.
- In Molecules 3-5 the mechanism of CS is the molecular wire -  $\beta$  is small which fits to this mechanism and the trend of "the longer the bridge the slower the rate" still works here but not as drastically as in the superexchange mechanism.
- (4) According to Marcus theory the maximum of the parabola = the Maximal  $K_{\text{ET}}$  will be achieved when  $-\Delta G = \lambda$ , before that  $K_{\text{ET}}$  grows when  $\Delta G$  (the driving force) grows. After that point ( $-\Delta G = \lambda$ ) we are approaching into the inverted region in which the increase of  $\Delta G$  vs  $\lambda$  will cause a reduction in reaction rate.  $[-\Delta G > \lambda]$ .
- A polar solvent would stabilize the CS state - that will happen due to the organization of the solvent molecules with their dipole moments toward the separated charges. This last move increases  $\lambda$  - and ~~effec~~ can facilitate the reaction.

(5a)  $\Delta G_{\text{CS}} = e(F_{\text{ox}}(D) - E_{\text{red}}(A)) - E_{\text{oo}} - \frac{e^2}{4\pi\epsilon_0\epsilon_r R_c} - S$

$$\Delta G_{\text{CS}} = 0.6 - (-0.6) - 2.2 \quad \text{no information}$$

$$\Delta G_{\text{CS}} \approx -1 \text{ eV}$$

$$E_{\text{oo}} = \frac{1242}{565 \text{ nm}} = 2.2 \text{ eV}$$

- b. According to the graph it is easy to see that  $n=1-3$  are drastically affected by the distance of D to A, which point out the superexchange regime, and after that  $n>3$  (4,5) there is a change in mechanism to the molecular wire - the rate increases with  $n$  - the more conjugated the bridge is the ~~the~~ electronic wave function has better compatibility with the D and hence the recombination rate increases.

$r_i = 0.2 \text{ nm} = u \times n$   
depending on the mass of A  
another we can say  
 $\Delta n_{\text{ion}} = n \mu (n-1)^{-1}$

since  $E_{\text{kinetic}} = \frac{1}{2} m v^2$   
we will get smaller gaps  
when we will use light atoms

shape of bridge  
will affect the reaction rate

light atoms

heavy atoms

bridge

concep

on

go

Nullikken said that as  
we will have a level of understanding that will be just  
right arrows

concept

on

go

concep

on

go

concep

on

go

concep

③b. It seems that in 1&2 the mechanism of CS is the superexchange mechanism.

It's easy to see that the longer the molecule the slower the reaction rate,

which fits to the dependency on D to A distance in this mechanism.

In Molecules 3-5 the mechanism of CS is the molecular wire -  $\beta$  is small  
which fits to this mechanism and the trend of "the longer the bridge the slower  
the rate" still works here but not as drastically as in the superexchange mechanism.

④ According to Markus theory the maximum of the parabola = the Maximal  $K_{\text{ET}}$   
will be achieved when  $-\Delta G = \lambda$ , before that  $K_{\text{ET}}$  grows when  $\Delta G$   
(the driving force) grows. After that point ( $-\Delta G = \lambda$ ) we are approaching into  
the inverted region in which the increase of  $-\Delta G$  vs  $\lambda$  will cause a reduction  
in reaction rate.  $[-\Delta G > \lambda]$ .

A polar solvent would stabilize the CS state - that will happen due to the  
organization of the solvent molecules with their dipole moments toward the  
separated charges. This last move increases  $\lambda$  - and ~~effec~~ can facilitate  
the reaction.

$$\text{⑤a. } \Delta G_{\text{CS}} = e \left( E_{\text{ox}}(D) - E_{\text{red}}(A) \right) - E_{\text{oo}} - \underbrace{\frac{e^2}{4\pi\epsilon_0 \epsilon_s R_c}}_{S} - S$$

$$\Delta G_{\text{CS}} = 0.6 - (-0.6) - 2.2 \quad \text{no information}$$

$$\Delta G_{\text{CS}} \approx -1 \text{ eV}$$

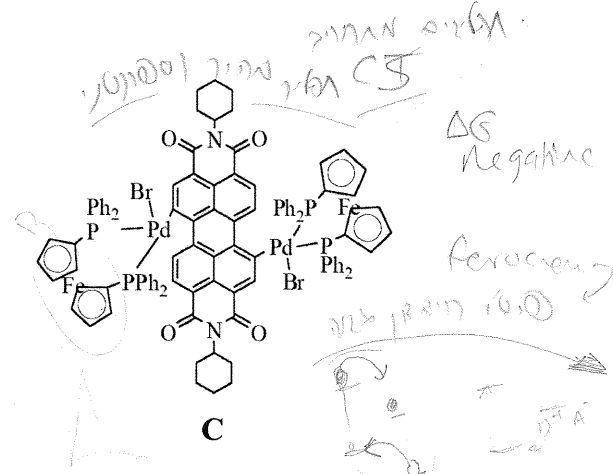
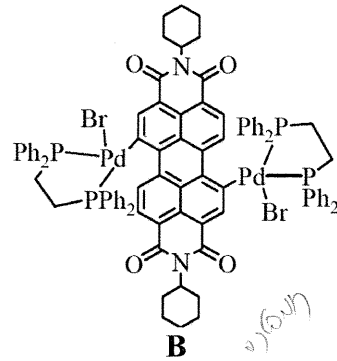
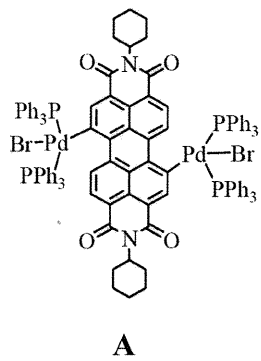
$$E_{\text{oo}} = \frac{1242}{565 \text{ nm}} = 2.2 \text{ eV}$$

b. According to the graph it is easy to see that  $n=1-3$  are drastically  
affected by the distance of D to A, which point out the superexchange  
regime, and after that  $n \geq 3$  (4,5) there is a change in mechanism  
to the molecular wire - the rate increases with  $n$  - the more conjugated  
the bridge is the ~~the~~ electronic wave function has better compatibility  
with the D and hence the recombination rate increases.

# Molecular Photonics

## Exercise 5

1. What is triplet harvesting in OLEDs? Why is it important, and how can one achieve it?
2. Consider the photosynthetic system of purple bacteria:
  - a. Describe the light harvesting function of the system.
  - b. Why do you think the flow of the electron in the reaction center is not symmetrical? Use the following link to help you to find the answer: [http://en.wikipedia.org/wiki/Photosynthetic\\_reaction\\_center](http://en.wikipedia.org/wiki/Photosynthetic_reaction_center)
3. Transient absorption  
Explain in **general** and include a scheme on how a transient absorption instrument works.
4. Case study I  
In the supplemental paper (Inorg. Chem. 2007, describes A and B) and in the lecture material (Elijah Shirman's presentation, describes A, B, and C) there are three PDI systems with different photophysical properties  
Explain shortly:
  - a. Why molecules A and B exhibit fluorescence
  - b. Why molecules A and B don't exhibit phosphorescence
  - c. Why molecule C does not show any emission, and explain in short how transient absorption helped in understanding the photophysics of C.



### 5. Case study II

- In the supplemental paper (JACS 2009) the reported molecule is aggregating in aqueous solutions.
- a. What can be said on the transition dipoles interactions in the aggregate according to its UV-vis spectrum?
  - b. What was learnt from the fluorescence studies of the aggregate?
  - c. What exciton mobility was found for the aggregate and how was it investigated?
  - d. Why photonic properties of the system are relevant to solar energy conversion?

## Palladium Complexes of Perylene Diimides: Strong Fluorescence Despite Direct Attachment of Late Transition Metals to Organic Dyes

Haim Weissman,<sup>†</sup> Elijah Shirman,<sup>†</sup> Tal Ben-Moshe,<sup>†</sup> Revital Cohen,<sup>‡</sup> Gregory Leitus,<sup>‡</sup> Linda J. W. Shimon,<sup>‡</sup> and Boris Rybtchinski<sup>\*,†</sup>

Department of Organic Chemistry and Chemical Research Support Unit, Weizmann Institute of Science, Rehovot 76100, Israel

Received March 21, 2007

We prepared the first  $\sigma$ -bonded metal complexes of widely utilized organic dyes, perylene tetracarboxylic acid diimides (PDIs). These 1,7-dipalladium PDI complexes were synthesized by C–Br oxidative addition of 1,7-dibromo-*N,N'*-dicyclohexyl PDI ( $\text{Br}_2\text{PDI}$ ) to  $\text{Pd}(0)$  phosphine complexes bearing triphenylphosphine and bischelating 1,2-bis(diphenylphosphino)ethane (dppe). The structures of Pd–PDI complexes were elucidated by single-crystal X-ray analysis. Surprisingly, despite direct attachment of two late transition metal centers, Pd–PDI systems are highly fluorescent ( $\Phi = 0.65$  and 0.22 for triphenylphosphine and dppe systems, respectively). This is rationalized in terms of weak electronic interactions between the metal centers and PDI  $\pi$ -system, as revealed by TD-DFT calculations.

Direct attachment of late transition metals to the aromatic systems of fluorescent organic chromophores entails unique structures and photofunction, yet the fluorescence is usually quenched due to efficient intersystem crossing.<sup>1</sup> This is due to enhanced spin–orbit coupling resulting from a heavy-atom effect induced by late transition metals. We show here that metal complexes based on perylene tetracarboxylic acid diimide (PDI) dyes, in which two palladium centers are attached to the dye aromatic core through metal–carbon  $\sigma$ -bonds, are highly fluorescent as a result of relatively weak electronic coupling between the metal-based orbitals and the dye  $\pi$ -system. Direct attachment of late transition metal centers to an organic dye, while maintaining high fluorescence, can represent an efficient tool for creating new structural and functional motifs, significantly augmenting the diversity of available photofunctional systems.

PDIs are widely utilized organic dyes.<sup>2</sup> They demonstrate exceptional thermal and photochemical stability, strongly absorb visible light, and show high fluorescence quantum

yields.<sup>3–5</sup> PDIs have been utilized as industrial dyes,<sup>2</sup> electronic materials,<sup>6–9</sup> sensors,<sup>10,11</sup> photovoltaics,<sup>12–16</sup> and building blocks for light-harvesting<sup>17–22</sup> and artificial photosynthetic systems.<sup>23</sup> While a variety of organic groups have been attached to the PDI core at the positions 1, 6, 7, and 12 (bay region),<sup>3</sup> direct attachment of transition metal centers to the PDI aromatic system has not been reported. Metal center and auxiliary ligand choice in such PDI derivatives would allow control over structure, photophysics, and self-

- (3) Würthner, F. *Chem. Commun.* 2004, 1564.
- (4) Langhals, H. *Helv. Chim. Acta* 2005, 88, 1309.
- (5) Wasielewski, M. R. *J. Org. Chem.* 2006, 71, 5051.
- (6) Struijk, C. W.; Sieval, A. B.; Dakhorst, J. E. J.; van Dijk, M.; Kimkes, P.; Koehorst, R. B. M.; Donker, H.; Schaafsma, T. J.; Picken, S. J.; van de Craats, A. M.; Warman, J. M.; Zuilhof, H.; Sudhölter, E. J. R. *J. Am. Chem. Soc.* 2000, 122, 11057.
- (7) Dimitrakopoulos, C. D.; Malenfant, P. R. L. *Adv. Mater.* 2002, 14, 99.
- (8) Jones, B. A.; Ahrens, M. J.; Yoon, M. H.; Facchetti, A.; Marks, T. J.; Wasielewski, M. R. *Angew. Chem., Int. Ed.* 2004, 43, 6363.
- (9) Yoo, B.; Jung, T.; Basu, D.; Dodabalapur, A.; Jones, B. A.; Facchetti, A.; Wasielewski, M. R.; Marks, T. J. *Appl. Phys. Lett.* 2006, 88, 082104/1.
- (10) Zang, L.; Liu, R.; Holman, M. W.; Nguyen, K. T.; Adams, D. M. J. *Am. Chem. Soc.* 2002, 124, 10640.
- (11) Wang, W.; Wan, W.; Zhou, H.-H.; Niu, S.; Li, A. D. Q. *J. Am. Chem. Soc.* 2003, 125, 5248.
- (12) Schmidt-Mende, L.; Fechtenkötter, A.; Müllen, K.; Moens, E.; Friend, R. H.; MacKenzie, J. D. *Science* 2001, 293, 1119.
- (13) Ego, C.; Marsitzky, D.; Becker, S.; Zhang, J.; Grimsdale, A. C.; Müllen, K.; MacKenzie, J. D.; Silva, C.; Friend, R. H. *J. Am. Chem. Soc.* 2003, 125, 437.
- (14) Yakimov, A.; Forrest, S. R. *Appl. Phys. Lett.* 2002, 80, 1667.
- (15) Breeze, A. J.; Salomon, A.; Ginley, D. S.; Gregg, B. A.; Tillmann, H.; Horhold, H. H. *Appl. Phys. Lett.* 2002, 81, 3085.
- (16) Shin, W. S.; Jeong, H.-H.; Kim, M.-K.; Jin, S.-H.; Kim, M.-R.; Lee, J.-K.; Leec, J. W.; Gal, Y.-S. *J. Mater. Chem.* 2006, 16, 384.
- (17) Qu, J.; Pschirer, N. G.; Liu, D.; Stefan, A.; Schryver, F. C. D.; Müllen, K. *Chem. Eur. J.* 2004, 10, 528.
- (18) Würthner, F.; You, C. C.; Saha-Möller, C. R. *Chem. Soc. Rev.* 2004, 33, 133.
- (19) Sautter, A.; Kaletas, B. K.; Schmid, D. G.; Dobrawa, R.; Zimine, M.; Jung, G.; van Stokkum, I. H. M.; De Cola, L.; Williams, R. M.; Würthner, F. *J. Am. Chem. Soc.* 2005, 127, 6719.
- (20) You, C. C.; Hippius, C.; Grune, M.; Würthner, F. *Chem. Eur. J.* 2006, 12, 7510.
- (21) Li, X. Y.; Sinks, L. E.; Rybtchinski, B.; Wasielewski, M. R. *J. Am. Chem. Soc.* 2004, 126, 10810.
- (22) Addicott, C.; Oesterling, I.; Yamamoto, T.; Müllen, K.; Stang, P. J. *J. Org. Chem.* 2005, 70, 797.
- (23) Rybtchinski, B.; Sinks, L. E.; Wasielewski, M. R. *J. Am. Chem. Soc.* 2004, 126, 12268.

\* To whom correspondence should be addressed. E-mail: boris.rybtchinski@weizmann.ac.il.

<sup>†</sup> Department of Organic Chemistry.

<sup>‡</sup> Chemical Research Support.

(1) Yersin, H.; Strasser, J. *Coord. Chem. Rev.* 2000, 208, 331.  
(2) Zollinger, H. *Color Chemistry*, 3rd ed.; VCH: Weinheim, 2003.

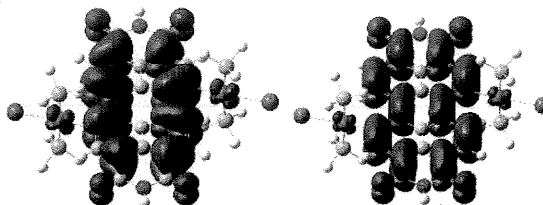


**Figure 4.** TD-DFT-derived contour surfaces of HOMO (right) and LUMO (left) for model system mimicking complex **1** (H imide substituents,  $\text{PH}_3$  ligands).

absorption and emission properties of complexes **1** and **2** remain unchanged in the presence of air. Overall, the position and vibronic structure of the emission peaks of **1** and **2** (small Stokes shifts, mirror image of absorption), independency of the emission on the presence of air, and short lifetimes suggest that the observed emission originates from the first excited singlet states. Femtosecond and nanosecond transient absorption studies employing 572-nm excitation (see Supporting Information) further confirm the formation of a  ${}^1\text{PDI}$  state, revealing its characteristic transient absorption peak in the spectra of **1** and **2**. The decay of  ${}^1\text{PDI}$  results in both fluorescence and intersystem crossing (as evidenced by the rise of PDI triplet bands, the triplet yield is 6% for **1** and 20% for **2**). Thus, our photophysical studies show that the *organopalladium PDIs are highly fluorescent*, unlike most complexes with metals directly attached to aromatic cores of organic chromophores.<sup>1</sup> Surprisingly, a heavy-atom effect is relatively moderate in  $\sigma$ -bonded Pd–PDI complexes, especially in the case of complex **1**.

In order to gain insight into the electronic structure of **1** and elucidate the nature of the heavy-atom effect induced by Pd centers, we performed TD-DFT calculations (B3LYP/SDB-cc-pVQZ//B3LYP/SDD level of theory) on a model system mimicking complex **1**, see Figure 4. Frontier molecular orbitals of the model system, HOMO and LUMO, are both localized on the PDI ligand, with minor participation of the Pd centers in the frontier orbitals makeup. Thus, in complex **1**,  $\sigma$ -bonds connecting two late transition metal centers with the chromophore core do not bring about strong interaction between the Pd orbitals and PDI  $\pi$ -system, localizing the electronic excitation mostly on the PDI ligand. Such electronic structure is expected to diminish the Pd heavy-atom effect.<sup>25,26</sup> Complex **2** demonstrates more efficient intersystem crossing than **1**, most probably because



**Figure 5.** TD-DFT-derived contour surfaces of HOMO (right) and LUMO (left) for model system mimicking complex **2** (H imide substituents,  $\text{H}_2\text{P}-(\text{CH}_2)_2-\text{PH}_2$  ligands).

of its different structure and orbital makeup, see Figure 5. The Pd  $d_{z^2}$  orbital, participating in the HOMO makeup of **2**, may introduce somewhat stronger electronic coupling between PDI and Pd. Yet, this does not bring about exclusive intersystem crossing, since complex **2** demonstrates a significant fluorescence quantum yield (22%). Notably, Pd–PDI complexes, in which metal centers are bonded through pyridine ligands attached at the PDI imide positions, show fluorescence quantum yields of 88%, indicating that the longer distances and weaker electronic coupling between Pd and PDI further diminish the heavy-atom effect.<sup>18</sup>

In conclusion, the first  $\sigma$ -bonded metal complexes, based on widely utilized in research and industry PDI dyes, have been synthesized and fully characterized. These complexes show unexpectedly strong fluorescence despite the fact that two late transition metals are directly attached to an aromatic system of the organic dye. This effect is due to relatively weak electronic coupling of Pd with the frontier  $\pi$ -orbitals of PDI. The structure and function of such complexes can be controlled by an auxiliary ligand choice. We believe that these findings will allow development of novel photofunctional systems based on PDI and transition metal complexes and provide guidelines for the control over photophysical characteristics of  $\sigma$ -bonded organometallic dyes.

**Acknowledgment.** This work was supported by grants from Sir Harry Djanogly, CBE, and the Weizmann Institute Alternative Energy Research Initiative. We thank Dr. Paramasivan Rajasingh for the synthesis of  $\text{Br}_2\text{PDI}$ . We thank Prof. M. R. Wasielewski, Mr. R. F. Kelley, and Ms. A. M. Vega (Northwestern University) for their assistance with transient absorption experiments. E.S. and H.W. acknowledge fellowships from the Feinberg Graduate School of the Weizmann Institute of Science. B.R. holds the Abraham and Jennie Fialkow Career Development Chair.

**Supporting Information Available:** Experimental and computational details; synthetic procedures and characterization; X-ray data (CIF); time-resolved data. This material is available free of charge via the Internet at <http://pubs.acs.org>.

IC700539B

- (25) Chandra, A. K.; Turro, N. J.; Lyons, A. L., Jr.; Stone, P. *J. Am. Chem. Soc.* **1978**, *100*, 4964.  
 (26) Kim, K.-Y.; Liu, S.; Kölse, M. E.; Schanze, K. S. *Inorg. Chem.* **2006**, *45*, 2509.

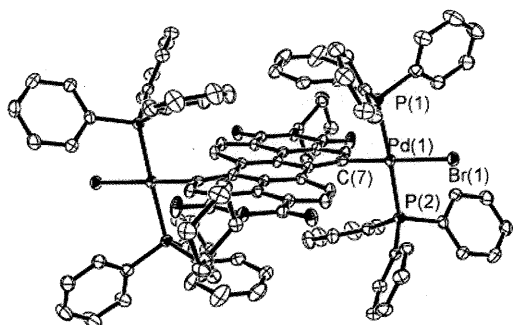
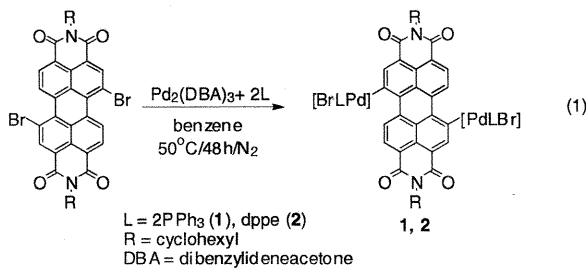


**Figure 1.** ORTEP drawing of complex **1**, 50% probability level. Hydrogen atoms and solvent molecules are omitted for clarity. Selected bond lengths ( $\text{\AA}$ ) and angles (deg): Pd(1)–C(7), 2.019(3); Pd(1)–P(1), 2.3607(8); Pd(1)–P(2), 2.3550(8); Pd(1)–Br(1), 2.5204(8); C(7)–Pd(1)–Br(1), 179.57(9); P(1)–Pd(1)–P(2), 172.12(3).

organization. We prepared *the first  $\sigma$ -bonded metal complexes of PDI employing oxidative addition of 1,7-dibromo-*N,N'*-dicyclohexyl PDI (Br<sub>2</sub>PDI)<sup>24</sup> to Pd(0) phosphine complexes prepared in situ (eq 1). We chose triphenylphos-*



phine and bischelating 1,2-bis(diphenylphosphino)ethane (dppe) ligands in order to study how changes in the Pd coordination sphere affect the structure and photophysical properties of Pd–PDI complexes.

Complexes **1** and **2** were characterized by multinuclear NMR spectroscopy, mass spectroscopy, UV-vis and fluorescence spectroscopy, electrochemistry, elemental analysis, and X-ray crystallography. <sup>31</sup>P{<sup>1</sup>H} NMR spectrum of complex **1** gives rise to a singlet centered at 20.9 ppm, consistent with trans arrangement of the phosphines. In complex **2**, the chelating ligand imposes cis configuration resulting in AX pattern in <sup>31</sup>P{<sup>1</sup>H} NMR spectrum exhibiting doublets at 36.3 and 50.9 ppm ( $J_{PP} = 28.5$  Hz). The <sup>1</sup>H NMR and <sup>13</sup>C{<sup>1</sup>H} NMR spectra confirm the different ligand coordination modes in **1** vs **2**. Notably, complexes **1** and **2** are stable for days in aerated solutions.

Further insight into the structure of **1** and **2** was obtained from X-ray crystallography. Single-crystal X-ray studies show that the auxiliary ligands choice has a pronounced effect on the structure, see Figures 1 and 2. X-ray analysis reveals that the phosphines in complex **1** are in a trans configuration, while in complex **2**, these are cis to each other, in agreement with the NMR studies. Complexes **1** and **2** have square planar geometry around the Pd centers. There is no significant change in the bond lengths of the PDI skeletons relative to Br<sub>2</sub>PDI, whose X-ray structure has been reported.<sup>24</sup> The central six-membered rings of the PDI moieties in **1**

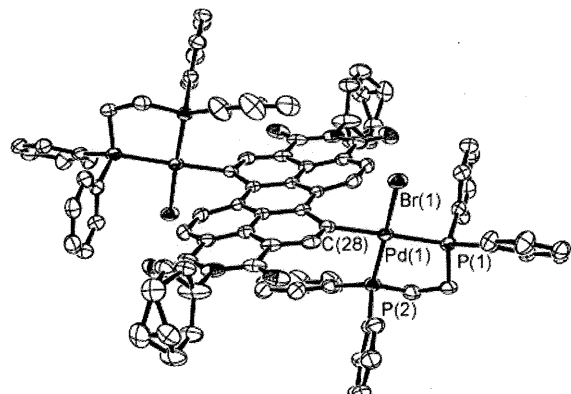


**Figure 2.** ORTEP drawing of complex **2**, 50% probability level. Hydrogen atoms and solvent molecules are omitted for clarity. Selected bond lengths ( $\text{\AA}$ ) and angles (deg): Pd(1)–C(28), 2.053(3); Pd(1)–P(1), 2.3355(9); Pd(1)–P(2), 2.251(1); Pd(1)–Br(1), 2.4980(7); C(28)–Pd(1)–P(1), 171.90(8); Br(1)–Pd(1)–P(2), 172.62(3).

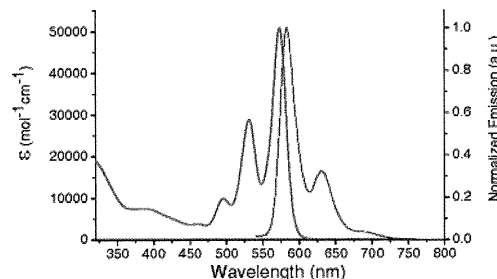


**Figure 3.** UV–vis (blue trace) and fluorescence (red trace) spectra of complex **1** in dichloromethane. Complex **2** shows very similar spectra.

and **2** are somewhat less twisted from planarity than in Br<sub>2</sub>PDI: the dihedral angles in the bay area are 12.1° and 17.3° for complexes **1** and **2**, respectively, compared to 24° in Br<sub>2</sub>PDI.<sup>24</sup> An intramolecular  $\pi$ – $\pi$  stacking motif is present in the crystal structures of **1** (four phenyl rings interact with the PDI  $\pi$ -system) and **2** (two phenyl rings interact with the PDI), see Figure 1. Interestingly, the crystal structure of **1** reveals that the PDI moiety is enclosed between the phenyl groups of the phosphine ligands, representing a novel, potentially useful structural motif for crystal engineering of PDI-based materials. Nuclear Overhauser effect (NOE) studies indicate that **1** and **2** do not show NOE attributable to  $\pi$ -stacking in solution.

UV–vis spectra of complexes **1** and **2** show similar absorption bands in dichloromethane peaked at 573 and 572 nm, respectively, with vibronic structure typical for S<sub>0</sub>–S<sub>1</sub> transition of PDI chromophores,<sup>3</sup> see Figure 3. It should be noted that the absorption bands of **1** and **2** are red-shifted by ca. 50 nm relative to unsubstituted PDIs ( $\lambda_{\text{max}} \approx 520$  nm).<sup>3</sup> Such a red-shift indicates that the Pd centers have electron-donating character (e.g., for diphenoxyl PDIs,  $\lambda_{\text{max}} \approx 550$  nm).<sup>3,5</sup> Complexes **1** and **2** show strong luminescence peaked at 584 nm, see Figure 3. The emission quantum yield of complex **1** is 65%, while the quantum yield of complex **2** is 22% in dichloromethane. In a less polar solvent such as benzene, **1** and **2** show absorption and emission spectra similar to those obtained in dichloromethane solution, indicating that the electronic transitions do not have significant charge-transfer character. The emission lifetimes are 7.5 and 2.8 ns for complexes **1** and **2**, respectively. The

(24) Würthner, F.; Stepanenko, V.; Chen, Z.; Saha-Möller, C. R.; Kocher, N.; Stalke, D. *J. Org. Chem.* 2004, 69, 7933.

## Supramolecular Gel Based on a Perylene Diimide Dye: Multiple Stimuli Responsiveness, Robustness, and Photofunction

Elisha Krieg,<sup>†</sup> Elijah Shirman,<sup>†</sup> Haim Weissman,<sup>†</sup> Eyal Shimon,<sup>‡</sup> Sharon G. Wolf,<sup>‡</sup>  
Iddo Pinkas,<sup>§</sup> and Boris Rybtchinski\*,<sup>†</sup>

Departments of Organic Chemistry, Plant Sciences, and Chemical Research Support,  
Weizmann Institute of Science, Rehovot 76100, Israel

Received May 14, 2009; E-mail: boris.rybtchinski@weizmann.ac.il

**Abstract:** Design of an extensive supramolecular three-dimensional network that is both robust and adaptive represents a significant challenge. The molecular system **PP2b** based on a perylene diimide chromophore (PDI) decorated with polyethylene glycol groups self-assembles in aqueous media into extended supramolecular fibers that form a robust three-dimensional network resulting in gelation. The self-assembled systems were characterized by cryo-TEM, cryo-SEM, and rheological measurements. The gel possesses exceptional robustness and multiple stimuli-responsiveness. Reversible charging of **PP2b** allows for switching between the gel state and fluid solution that is accompanied by switching on and off the material's birefringence. Temperature triggered deswelling of the gel leads to the (reversible) expulsion of a large fraction of the aqueous solvent. The dual sensibility toward chemical reduction and temperature with a distinct and interrelated response to each of these stimuli is pertinent to applications in the area of adaptive functional materials. The gel also shows strong absorption of visible light and good exciton mobility (elucidated using femtosecond transient absorption), representing an advantageous light harvesting system.

### Introduction

Gels are exceptionally versatile materials.<sup>1–4</sup> In particular, stimuli-responsive gels are of great importance for the development of adaptive multifunctional systems (smart materials).<sup>5–10</sup> It has been demonstrated that some gels respond to temperature,<sup>11,12</sup> redox agents<sup>13–16</sup> and other chemical entities,<sup>17,18</sup> electric field,<sup>19</sup>

light,<sup>20–24</sup> and sound.<sup>25</sup> A response to multiple stimuli has also been demonstrated.<sup>26–28</sup> Multiple stimuli-responsiveness is especially beneficial for creation of smart materials.<sup>29,30</sup>

Supramolecular gels that are composed of small molecules held together by noncovalent interactions possess advantageous properties for creation of responsive materials due to the dynamic character of noncovalent bonding.<sup>5</sup> Such gels are based

- <sup>†</sup> Department of Organic Chemistry.  
<sup>‡</sup> Department of Chemical Research Support.  
<sup>§</sup> Department of Plant Sciences.
- (1) Sangeetha, N. M.; Maitra, U. *Chem. Soc. Rev.* **2005**, *34*, 821–836.  
(2) Hirst, A. R.; Escuder, B.; Miravet, J. F.; Smith, D. K. *Angew. Chem., Int. Ed.* **2008**, *47*, 8002–8018.  
(3) Xie, P.; Zhang, R. J. *Mater. Chem.* **2005**, *15*, 2529–2550.  
(4) Maeda, S.; Hara, Y.; Sakai, T.; Yoshida, R.; Hashimoto, S. *Adv. Mater.* **2007**, *19*, 3480–3484.  
(5) Jong, J.; Feringa, B.; Esch, J. Responsive Molecular Gels. In *Molecular Gels: Materials with Self-Assembled Fibrillar Networks*; Weiss, R. G., Terech, P., Eds.; Springer: Dordrecht, 2006; pp 895–927.  
(6) Maeda, H. *Chem.—Eur. J.* **2008**, *14*, 11274–11282.  
(7) Hendrickson, G. R.; Lyon, L. A. *Soft Matter* **2009**, *5*, 29–35.  
(8) Ahn, S. K.; Kasi, R. M.; Kim, S. C.; Sharma, N.; Zhou, Y. X. *Soft Matter* **2008**, *4*, 1151–1157.  
(9) Ishii, T.; Shinkai, S. *Top. Curr. Chem.* **2005**, *258*, 119–160.  
(10) Sidorenko, A.; Krupenkin, T.; Taylor, A.; Fratzl, P.; Aizenberg, J. *Science* **2007**, *315*, 487–490.  
(11) Yoshida, R.; Uchida, K.; Kaneko, Y.; Sakai, K.; Kikuchi, A.; Sakurai, Y.; Okano, T. *Nature* **1995**, *374*, 240–242.  
(12) Kiyonaka, S.; Sugiyasu, K.; Shinkai, S.; Hamachi, I. *J. Am. Chem. Soc.* **2002**, *124*, 10954–10955.  
(13) Kawano, S.-i.; Fujita, N.; Shinkai, S. *J. Am. Chem. Soc.* **2004**, *126*, 8592–8593.  
(14) Chen, J.; McNeil, A. J. *J. Am. Chem. Soc.* **2008**, *130*, 16496–16497.  
(15) Tomatsu, I.; Hashidzume, A.; Harada, A. *Macromol. Rapid Commun.* **2006**, *27*, 238–241.  
(16) Wang, C.; Zhang, D.; Zhu, D. *J. Am. Chem. Soc.* **2005**, *127*, 16372–16373.
- (17) Deng, W.; Yamaguchi, H.; Takashima, Y.; Harada, A. *Angew. Chem., Int. Ed.* **2007**, *46*, 5144–5147.  
(18) Kim, H.-J.; Lee, J.-H.; Lee, M. *Angew. Chem., Int. Ed.* **2005**, *44*, 5810–5814.  
(19) Mizoshita, N.; Suzuki, Y.; Kishimoto, K.; Hanabusa, K.; Kato, T. *J. Mater. Chem.* **2002**, *12*, 2197–2201.  
(20) Guerzo, A.; Pozzo, J.-L. Photoresponsive Gels. In *Molecular Gels: Materials with Self-Assembled Fibrillar Networks*; Weiss, R. G., Terech, P., Eds.; Springer: Dordrecht, 2006; pp 817–855.  
(21) Matsumoto, S.; Yamaguchi, S.; Ueno, S.; Komatsu, H.; Ikeda, M.; Ishizuka, K.; Iko, Y.; Tabata, K. V.; Aoki, H.; Ito, S.; Noji, H.; Hamachi, I. *Chem.—Eur. J.* **2008**, *14*, 3977–3986.  
(22) Peng, F.; Li, G.; Liu, X.; Wu, S.; Tong, Z. *J. Am. Chem. Soc.* **2008**, *130*, 16166–16167.  
(23) Sumaru, K.; Ohi, K.; Takagi, T.; Kanamori, T.; Shinbo, T. *Langmuir* **2006**, *22*, 4353–4356.  
(24) Akazawa, M.; Uchida, K.; de Jong, J. J. D.; Areephong, J.; Stuart, M.; Caroli, G.; Browne, W. R.; Feringa, B. L. *Org. Biomol. Chem.* **2008**, *6*, 1544–1547.  
(25) Naota, T.; Koori, H. *J. Am. Chem. Soc.* **2005**, *127*, 9324–9325.  
(26) Weng, W.; Beck, J. B.; Jamieson, A. M.; Rowan, S. J. *J. Am. Chem. Soc.* **2006**, *128*, 11663–11672.  
(27) Liu, J.; He, P.; Yan, J.; Fang, X.; Peng, J.; Liu, K.; Fang, Y. *Adv. Mater.* **2008**, *20*, 2508–2511.  
(28) Komatsu, H.; Matsumoto, S.; Tamaru, S.-i.; Kaneko, K.; Ikeda, M.; Hamachi, I. *J. Am. Chem. Soc.* **2009**, *131*, 5580–5585.  
(29) Yerushalmi, R.; Scherz, A.; van der Boom, M. E.; Kraatz, H.-B. *J. Mater. Chem.* **2005**, *15*, 4480–4487.  
(30) Yoshida, M.; Lahann, J. *ACS Nano* **2008**, *2*, 1101–1107.

on self-assembly of molecular subunits into one-dimensional fibers<sup>31,32</sup> that further assemble into a three-dimensional network. As the structure of supramolecular gels is determined by a hierarchy of various structural elements, their response can take place on different structural levels.<sup>33–35</sup> Importantly, most supramolecular gels are characterized by a gel to sol transition at moderate temperatures as the strength of noncovalent bonding is comparable to ambient thermal energy.<sup>5</sup> Thus, although very advantageous as regards stimuli responsiveness, supramolecular gels lack robustness. In general, design of an extensive supramolecular three-dimensional network that is both robust<sup>36</sup> and adaptive represents a significant challenge.

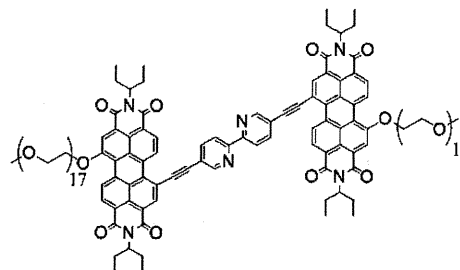
Water is an advantageous medium for self-assembly,<sup>37</sup> which is characterized by strong hydrophobic forces when extended hydrophobic surfaces are involved.<sup>38–40</sup> At the same time, reversible attenuation of hydrophobicity is feasible and can lead to a high degree of adaptivity. We have recently demonstrated that reversible depolymerization of supramolecular polymers assembled in aqueous medium can be achieved through charging/discharging of the aromatic subunits.<sup>41</sup> Hence, *supramolecular hydrogels based on extended aromatic systems* can result in both robust and responsive (through aromatic charging) networks. In addition, such gels, if based on chromophores, should have advantageous photonic and electronic characteristics. For example, supramolecular gels based on dyes have been found to possess excellent light harvesting properties.<sup>1,9,42</sup> Recent examples include organogels based on  $\pi$ -conjugated molecular systems such as oligo(phenylenevinylene)s,<sup>42–44</sup> platinum acetylide oligomers,<sup>45</sup> and perylene diimides.<sup>46–48</sup> In contrast to these *organogels*, the area of light harvesting *hydrogels* is largely unexplored.<sup>49,50</sup>

Herein we report on a supramolecular perylene diimide-based gel, which assembles due to hydrophobic interactions. It is

robust, yet adaptive (demonstrates multiple stimuli-responsiveness), and possesses advantageous light harvesting properties.

## Results and Discussion

Following our interest in the self-assembly of nanoscale photofunctional systems in an aqueous medium,<sup>41,57</sup> we have synthesized compound **PP2b** (synthesis and characterization are described in the Supporting Information). **PP2b** is based on a perylene diimide (PDI) chromophore that is known for its exceptional thermal and photochemical stability, strong absorption of visible light, and high fluorescence quantum yields.<sup>51,52</sup> The extended  $\pi$ -conjugated core of **PP2b** containing PDI, bipyridyl, and ethynyl moieties is strongly hydrophobic, while hydrophilic polyethylene glycol (PEG) side chains result in overall amphiphilicity of **PP2b**. The bipyridyl (bipy) linker was chosen because of its planar structure. Thus, **PP2b** possesses an extended flat aromatic core with a strong propensity for stacking and enhanced hydrophobicity. Upon stacking of **PP2b** in an aqueous medium several new hydrophobic (or partially hydrophobic) interfaces may develop,<sup>41,57</sup> leading to a hierarchical multidimensional character of assembly. Additionally, bipy is a good ligand for a variety of metals, making it possible to tune the **PP2b** structure and properties via metal coordination. This represents a subject of future studies.



PP2b

**PP2b** is disaggregated in various organic solvents, such as chloroform, dichloromethane, and THF, showing sharp visible light absorption bands, strong fluorescence, and sharp peaks in the NMR spectrum (see Figures S1, S2). Self-assembly of **PP2b** is induced by addition of water to a solution of the compound in THF. UV/vis spectroscopy of **PP2b** in different water/THF mixtures indicates aggregation (Figure 1). Thus, increasing water content leads to broadening of the absorption bands, accompanied by some loss of absorption intensity, a slight red shift, and an inversion of relative intensities of 0–0 and 0–1 electronic transitions, typical of face-to-face stacking of PDI molecules.<sup>51</sup> In a disaggregating solvent such as THF, **PP2b** shows strong fluorescence ( $\lambda_{\text{max}} = 603 \text{ nm}$ , quantum yield = 58%) that is quenched upon addition of water (Figure S3). In solutions containing 20 vol% THF content or less, fluorescence is quenched almost quantitatively, indicating a high degree of aggregation. The very low residual fluorescence of **PP2b** in this solvent mixtures is red-shifted ( $\lambda_{\text{max}} = 685 \text{ nm}$ ), characteristic of excimer fluorescence.<sup>53</sup> The water/THF mixtures of **PP2b** are homogeneous and stable over time as long as the THF content is above 10 vol%. Below this content the mixture

- (31) Schenning, A. P. H. J.; Meijer, E. W. *Chem. Commun.* **2005**, 3245–3258.

(32) Zang, L.; Che, Y.; Moore, J. S. *Acc. Chem. Res.* **2008**, *41*, 1596–1608.

(33) Estroff, L. A.; Hamilton, A. D. *Chem. Rev.* **2004**, *104*, 1201–18.

(34) Hecht, S. *Mater. Today* **2005**, 48–55.

(35) Elemans, J. A. A. W.; Rowan, A. E.; Nolte, R. J. M. *J. Mater. Chem.* **2003**, *13*, 2661–2670.

(36) Diaz, D. D.; Cid, J. J.; Vazquez, P.; Torres, T. *Chem.—Eur. J.* **2008**, *14*, 9261–9273.

(37) Oshovsky, G. V.; Reinhoudt, D. N.; Verboom, W. *Angew. Chem., Int. Ed.* **2007**, *46*, 2366–2393.

(38) Meyer, E. A.; Castellano, R. K.; Diederich, F. *Angew. Chem., Int. Ed.* **2003**, *42*, 1210–1250.

(39) Chandler, D. *Nature* **2005**, *437*, 640–647.

(40) Ball, P. *Chem. Rev.* **2008**, *108*, 74–108.

(41) Baram, J.; Shirman, E.; Ben-Shitrit, N.; Ustinov, A.; Weissman, H.; Pinkas, I.; Wolf, S. G.; Rybtchinski, B. *J. Am. Chem. Soc.* **2008**, *130*, 14966–14967.

(42) Ajayaghosh, A.; Praveen, V. K.; Vijayakumar, C. *Chem. Soc. Rev.* **2008**, *37*, 109–22.

(43) Ajayaghosh, A.; George, S. J.; Praveen, V. K. *Angew. Chem., Int. Ed.* **2003**, *42*, 332–335.

(44) van Herrikhuizen, J.; George, S. J.; Vos, M. R. J.; Sommerdijk, N. A. J. M.; Ajayaghosh, A.; Meskers, S. C. J.; Schenning, A. P. H. J. *Angew. Chem., Int. Ed.* **2007**, *46*, 1825–1828.

(45) Cardolaccia, T.; Li, Y.; Schanze, K. S. *J. Am. Chem. Soc.* **2008**, *130*, 2535–2545.

(46) Sugiyasu, K.; Fujita, N.; Shinkai, S. *Angew. Chem.* **2004**, *116*, 1249–1253.

(47) Würthner, F.; Bauer, C.; Stepanenko, V.; Yagai, S. *Adv. Mater.* **2008**, *20*, 1695–1698.

(48) Würthner, F.; Hanke, B.; Lysetska, M.; Lambright, G.; Harms, G. S. *Org. Lett.* **2005**, *7*, 967–970.

(49) Nakashima, T.; Kimizuka, N. *Adv. Mater.* **2002**, *14*, 1113–1116.

(50) Montalti, M.; Dolci, L. S.; Prodi, L.; Zaccheroni, N.; Stuart, M. C. A.; van Bommel, K. J. C.; Friggeri, A. *Langmuir* **2006**, *22*, 2299–2303.

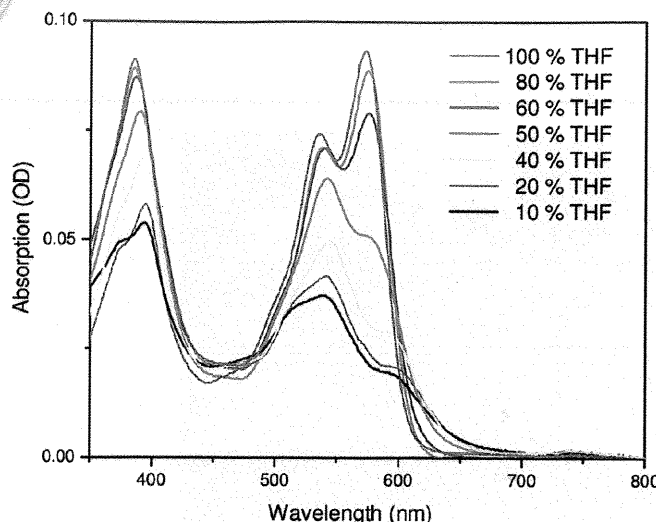


**Figure 1.** UV-vis spectrum of **PP2b** ( $2.4 \times 10^{-6}$  M) in THF and different water/THF mixtures.

becomes inhomogeneous and **PP2b** precipitates. We will denote homogeneous solutions of **PP2b** in water/THF mixtures with a large water content ( $\geq 80$  vol%) as “*aggregated solutions*”, whereas the term “*disaggregated solution*” is used to refer exclusively to solutions in organic solvents such as THF and chloroform. As discussed below, aggregated solutions become very viscous at concentrations above  $10^{-3}$  M and gelation is observed above a critical gel concentration (cgc) of  $\sim 6 \times 10^{-3}$  M. Therefore, when referring to **PP2b** at the cgc or above, the term “*supramolecular gel*” or just “*gel*” is used.

Cryogenic transmission electron microscopy (cryo-TEM) of water/THF solutions (80:20, v/v) of **PP2b** reveals the presence of uniform fibrous structures (Figure 2a,b). The width of the fibers is  $3.3 \pm 0.4$  nm, while they reach remarkable lengths of 1  $\mu$ m or more. The fibers form ordered structures, as manifested by alternating dark high-contrast regions separated by regular spacings of  $3.9 \pm 0.4$  nm. The darker-contrast regions represent tightly stacked conjugated systems that possess high electron density, while the lighter-contrast spacings represent a solvated shell of hydrophilic PEG tails.<sup>54</sup> The total width of a single fiber (inner aromatic core region and outer PEG shell) is  $7.2 \pm 0.8$  nm. Upon increase in concentration, denser ordered structures are observed (Figure 2b). Individual fibers consist of segments of  $2.0 \pm 0.3$  nm height (Figure 2b, arrow), representing a rare example of segmented supramolecular fibers,<sup>55,56</sup> which we have also observed in several PDI-based self-assembled systems.<sup>41,57</sup> The width of the nanofibers appears to be uniform over a wide range of concentrations ( $1.7 \times 10^{-5}$ – $3.3 \times 10^{-3}$  M). Figure 2c shows the possible structure of the supramolecular fibers, based on molecular modeling (see Supporting Information).

In addition to their remarkable aspect ratio and high degree of organization, the nanofiber assemblies appear to form large mechanically stable structures, as they can be filtered off from the water/THF solution (80:20, v/v) using standard PTFE syringe

filters with a 0.2  $\mu$ m pore size (Figure 3a). The filtrate is colorless, indicating essentially quantitative removal of the dye aggregates. Further evidence supporting the formation of extended structures in solution was gained from an experiment, in which a layer of water/THF mixture (80:20, v/v) was carefully added on top of a  $10^{-4}$  M solution of **PP2b** in the same solvent, and the system was monitored to document mixing (Figure 3b–d). The photographs show the samples after 1 min (b), 6 h (c) and 4 days (d), indicating that almost no mixing is observed on the time scale of several days. Interestingly, such “nonmixing” behavior is typical of fully swelled gels, where addition of a solvent does not change the gel volume,<sup>58</sup> suggesting that **PP2b** forms a gel-like three-dimensional supramolecular network in aqueous solution.

Further insight into the solution-phase structure was obtained using cryogenic scanning electron microscopy (cryo-SEM, see Supporting Information for details), which is a methodology of choice for studying solvated three-dimensional networks.<sup>59,60</sup> Cryo-SEM images reveal that in a fluid aggregated solution the nanofibers form an interconnected three-dimensional network (Figure 4). The majority of the fibers have widths of  $6.5 \pm 1.0$  nm. Subtracting the thickness of the metal layer used for the imaging ( $\sim 0.6$  nm), the actual fiber width is  $5.9 \pm 1.0$  nm, corresponding to the  $7.2 \pm 0.8$  nm fiber width observed in cryo-TEM. The slightly smaller width observed in cryo-SEM can be due to a shrinkage of the PEG shell around the fibers caused by the sublimation of solvent from the vitrified gel during sample preparation (see Supporting Information).

**Supramolecular Gel.** In water/THF mixtures that contain between 10 and 20 vol% THF, **PP2b** forms gels above the critical gel concentration (cgc =  $6 \times 10^{-3}$  M), as evidenced by the rheological data (Figure 5) and vial inversion test (Figure 6a, inset). The gel was prepared by dissolving **PP2b** in THF in a vial, followed by the quick addition of water and vigorous shaking of the sample. Gelation takes place instantaneously. Rheological measurements reveal an elastic response; i.e., the storage modulus is larger than the loss modulus ( $G' \gg G''$ ), and a pronounced plateau region of these moduli plotted against the frequency (Figure 5a), which is a characteristic feature of gels.<sup>61</sup> The moduli are invariant over a wide range of strain (Figure 5b), revealing the gel response as a solid material even under large deformations.<sup>61</sup>

Once prepared, the gel is stable at room temperature in the presence of air and can be stored for several months without showing any change. The gel structure was studied by cryo-SEM, revealing an interconnected porous structure (Figure 6a) in which nanofibers create a three-dimensional network (Figure 6b). The smallest fibers have widths of  $6.1 \pm 1.1$  nm, and their actual width (subtracting the thickness of the metal layer used for gel imaging ( $\sim 0.6$  nm)) is  $5.5 \pm 1.1$  nm, similar to the size observed in the case of the solution-phase network. Furthermore, thicker fibers with various diameters have been observed, frequently branching out into smaller fibers. An additional distinctive characteristic is the presence of whirls and streams (Figure 6c,d). These anisotropic regions are several micrometers large and demonstrate a certain long-range order of the

- (55) Cui, H.; Chen, Z.; Zhong, S.; Wooley, K. L.; Pochan, D. J. *Science* **2007**, *317*, 647–650.
- (56) Li, Z.; Kesselman, E.; Talmon, Y.; Hillmyer, M. A.; Lodge, T. P. *Science* **2004**, *306*, 98–101.
- (57) Golubkov, G.; Weissman, H.; Shirman, E.; Wolf, S. G.; Pinkas I.; Rybtchinski, B. *Angew. Chem., Int. Ed.* **2009**, *48*, 926–930.

- (58) Yamauchi, A. Gels: Introduction. In *Gels Handbook*; Osada, Y., Kajiwara, K., Eds.; Academic: London, 2001; pp 4–12.
- (59) Matzelle, T.; Reichelt, R. *Acta Microscopica* **2008**, *17*, 45–61.
- (60) Menger, F. M.; Seredyuk, V. A.; Apkarian, R. P.; Wright, E. R. *J. Am. Chem. Soc.* **2002**, *124*, 12408–12409.
- (61) Kavanagh, G. M.; Ross-Murphy, S. B. *Prog. Polym. Sci.* **1998**, *23*, 533–562.

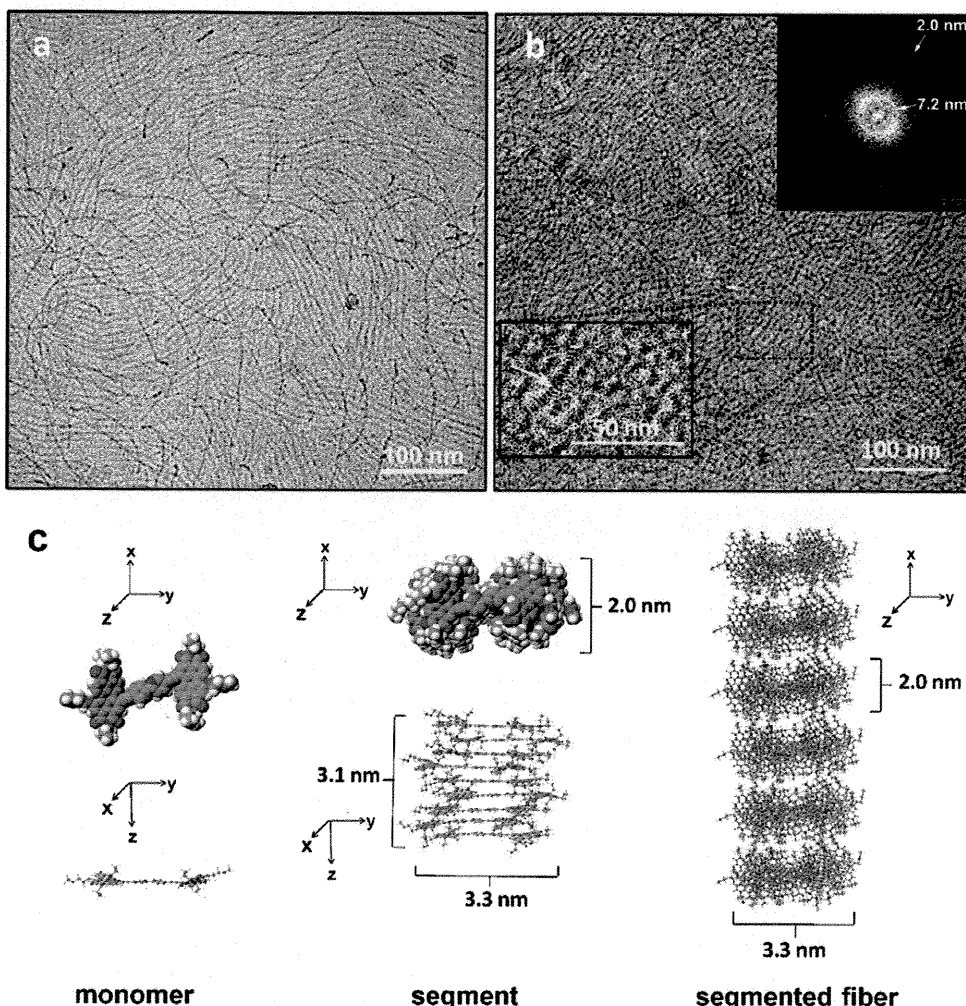


**Figure 2.** (a) Cryo-TEM image of **PP2b** aggregated solution ( $10^{-4}$  M) in water/THF mixture (80:20, v/v). The image shows ordered fibers (high contrast cores:  $3.3 \pm 0.4$  nm, low contrast spacings:  $3.9 \pm 0.4$  nm). (b) Cryo-TEM image of **PP2b** at higher concentration ( $3.3 \times 10^{-3}$  M). Some individual fibers show distinct segments (yellow arrow). Inset: FFT calculation showing spacing of 7.2 nm (fiber–fiber distance) and 2.0 nm (segment–segment distance). (c) Molecular modeling of **PP2b** and its supramolecular structures. For simplification, PEG chains are modeled as the  $-\text{O}(\text{CH}_2-\text{CH}_2)\text{OCH}_3$  group. Geometry optimization of the **PP2b** monomer was performed using the semiempirical PM3 method. The geometry of an individual segment and of the segmented fiber was optimized using the MM3 force field.

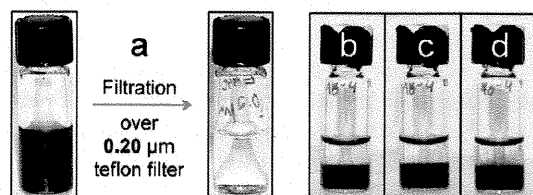


**Figure 3.** (a) Filtration experiment. The  $10^{-4}$  M solution of **PP2b** was filtered over a PTFE syringe filter with  $0.2\text{ }\mu\text{m}$  pore size. (b–d) Mixing experiment. A layer of water/THF mixture (80:20) was added on top of the aggregated solution of **PP2b** ( $10^{-4}$  M) in the same solvent mixture. The pictures are taken after (b) 1 min, (c) 6 h, and (d) 4 days.

supramolecular fibers within the gel. The structural anisotropies cause birefringence, as evidenced by polarized light microscopy (Figure 7). The observed morphologies and fiber widths are very similar in freshly prepared gel samples and in samples aged for a week, as observed in cryo-SEM images (Figure S5), consistent with rheological measurements that show a very similar elastic response in two samples.

UV-vis absorption spectra of the gel and aggregated solutions do not show a significant difference (Figure 8), confirming that the stacking geometry of the aromatic systems of **PP2b** is

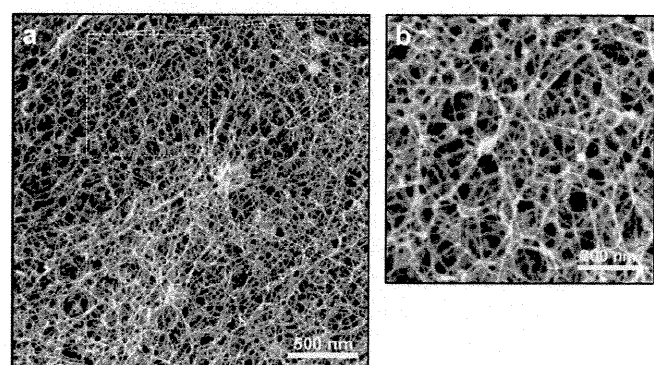


**Figure 4.** cryo-SEM images of an aggregated solution of **PP2b** ( $10^{-4}$  M) in water/THF mixture (80:20, v/v). (a) Extended network structure spanned by supramolecular fibers. (b) Magnified area. Individual fibers are  $6.5 \pm 1.0$  nm in diameter.

identical in solution and in gel, as expected from the overall similarity of the solution-phase and gel morphology. The main difference between the gel and solution network structures is the density of the network and, in particular, the thickness of the fibers. Thus, while the solution-phase network is built mainly

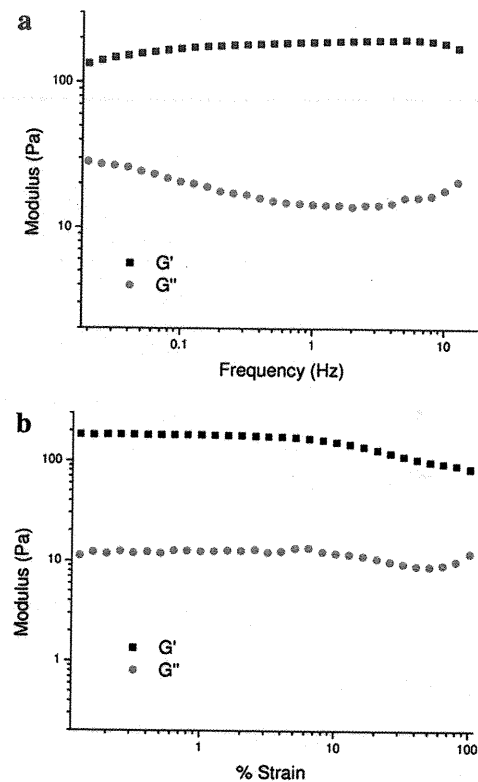


**Figure 5.** (a) Storage modulus,  $G'$ , and loss modulus,  $G''$ , as functions of frequency, measured at 2% strain. (b)  $G'$  and  $G''$  vs strain response measured at 1 Hz frequency.

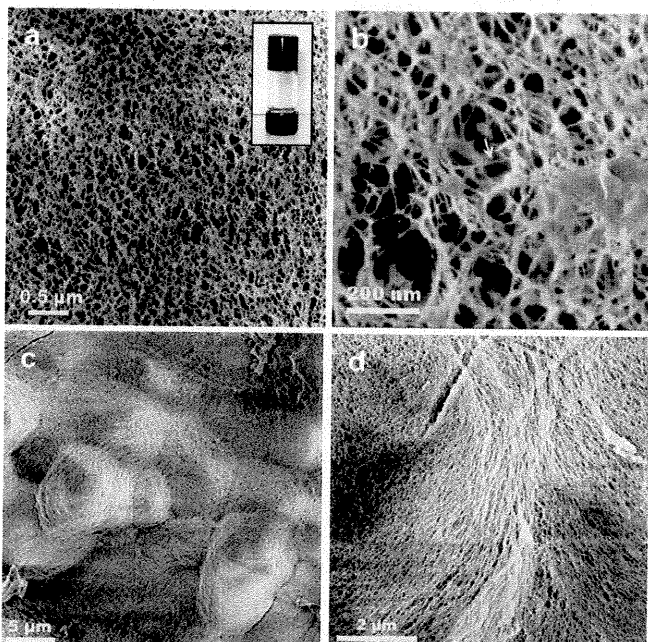


**Figure 6.** Cryo-SEM images of the gel of **PP2b** ( $8 \times 10^{-3}$  M, water/THF mixture (80:20)) at different magnifications. (a) Nanoporous structure of the three-dimensional network. Inset: vial inversion test. (b) Image at high magnification shows three-dimensional network of nanofibers. The smallest fibers are  $6.1 \pm 1.1$  nm in diameter (yellow arrow). (c) Whirls with diameters of 10–15  $\mu\text{m}$ . (d) Directional arrangement of fibers within a "microstream" in the gel.

from individual fibers and their thin bundles, the gel contains essentially thicker fiber bundles (Figures 4, 6), accounting for the greater mechanical strength of the gel.

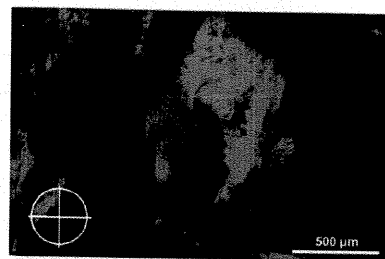


**Figure 7.** Polarized light microscopic image of the gel of **PP2b** ( $8 \times 10^{-3}$  M) in water/THF mixture (80:20, v/v). The white cross indicates the orientations of the polarizing filters.

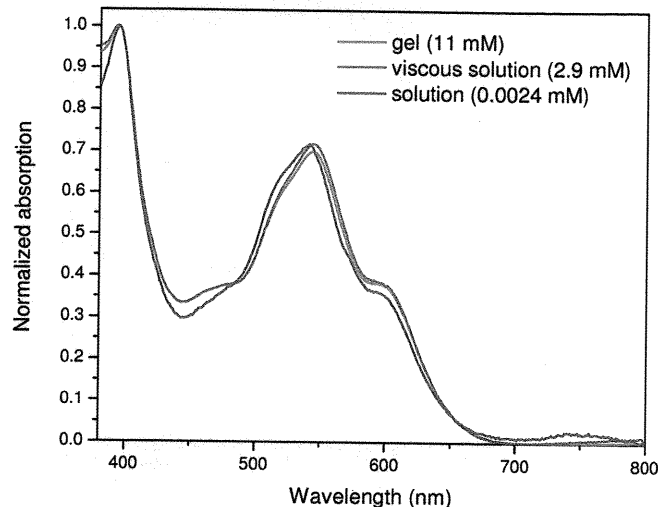


**Figure 8.** Normalized UV-vis absorption spectra of **PP2b** in water/THF mixture (80:20, v/v) at different concentrations, corresponding to gel (green trace), viscous solution (red trace), and dilute solution (blue trace).

We anticipate that the structure of the supramolecular fibers in both gel and solution follows the same hierarchy of self-assembly. The proposed assembly sequence, schematically depicted in Figure 9, is based on molecular modeling studies (Figure 2c) and electron microscopy data. On a first hierarchical level, the hydrophobic effect and  $\pi-\pi$  interactions cause face-to-face stacking of **PP2b** into small aggregates of 8–10 molecules. Stacked molecules are shifted in respect to each other, due to the steric bulk of the ethylpropyl substituents attached to the imides in PDI. On a second hierarchical level, the hydrophobic effect is the driving force for further aggregation, this time driven by the aliphatic side chains of PDI imide substituents that, as a result of PDI stacking, form a substantial hydrophobic domain. Their interaction results in fibers with distinct segmentation. Then the fibers assemble into entangled bundles.<sup>49</sup> Branching out of these might provide a mechanism for the creation of junctions.<sup>62</sup> Strong interactions between the fibers are most probably due to the significant residual hydrophobicity of the fiber interface.

**Stimuli-Responsiveness.** PDI systems are prone to reduction, some of them forming stable mono- and dianions in an aqueous medium<sup>63,64</sup> that can be converted back to neutral PDI upon exposure to air.<sup>63</sup> We have recently shown that this aromatic charge/discharge cycle can be utilized for reversible depolymerization of supramolecular polymers.<sup>41</sup>

- (62) Keller, A. *Faraday Discuss.* **1995**, *101*, 1–49.
- (63) Shirman, E.; Ustinov, A.; Ben-Shitrit, N.; Weissman, H.; Iron, M. A.; Cohen, R.; Rybtchinski, B. *J. Phys. Chem. B* **2008**, *112*, 8855–8858.
- (64) Marcon, R. O.; Brochstain, S. *J. Phys. Chem. A* **2009**, *113*, 1747–1752.

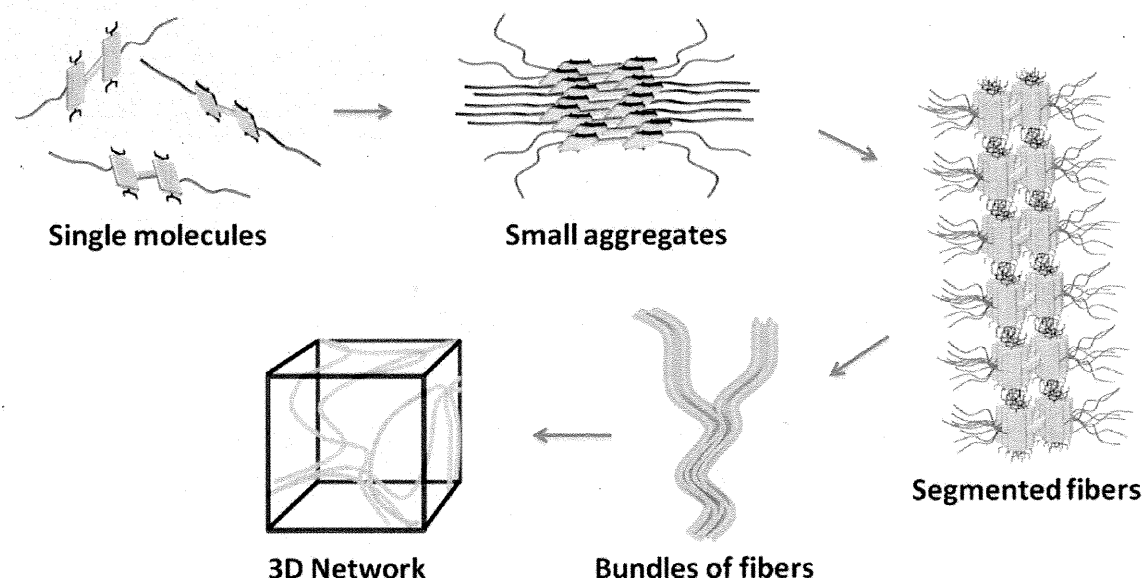


**Figure 9.** Schematic illustration of the PP2b assembly hierarchy.

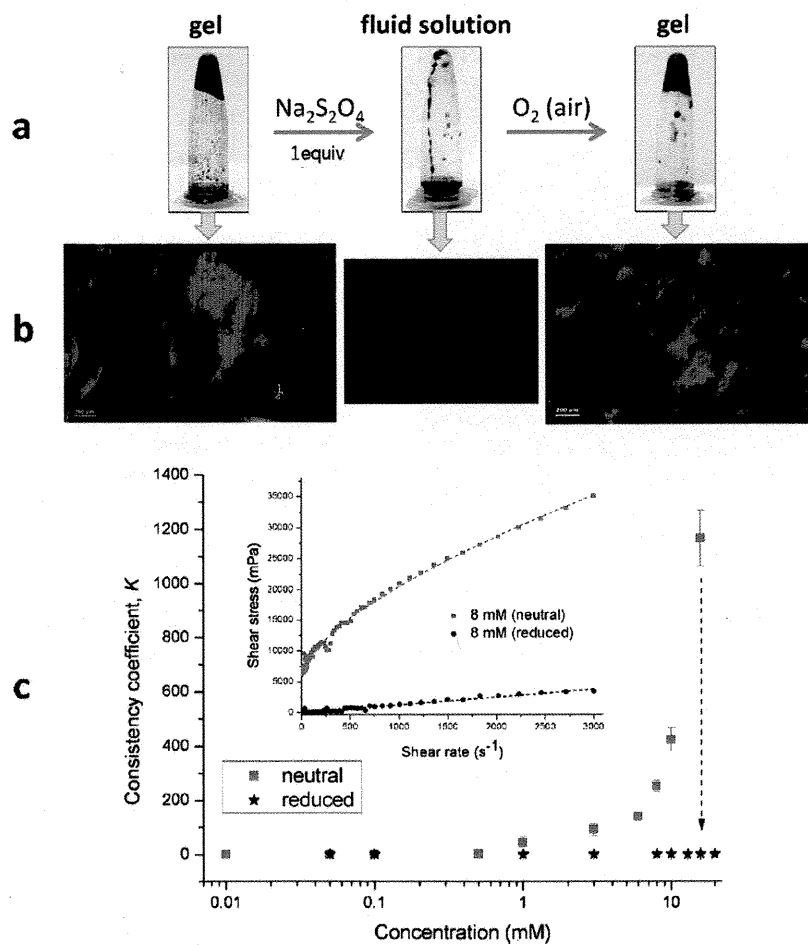


**Figure 10.** Effect of reversible charging of the gel in water/THF mixture (85:15, v/v). (a) Inverted tubes of the gel ( $8 \times 10^{-3}$  M) before reduction, after reduction with 1 equiv of  $\text{Na}_2\text{S}_2\text{O}_4$ , and after oxidation back to the neutral state using air. (b) Polarized light microscopic images of the corresponding samples. (c) Plot of the consistency coefficient  $K$  as a function of the concentration of PP2b in water/THF mixture (85:15) for the neutral form (red) and the reduced form (black). The reduced samples are always fluid solutions. Inset: An example of a plot of shear rate vs shear stress for neutral sample and reduced sample ( $8 \times 10^{-3}$  M).

Addition of an aqueous solution of 1 equiv of sodium dithionite to the supramolecular gel under an inert atmosphere causes a dramatic loss of viscosity, creating a fluid solution within several seconds (gel to sol transition, Figure 10). Ex-

posure of the resultant solution to air restores the gel within 10 min. The process is reversible and can be repeated at least three times. The transition of the gel to the fluid solution by reduction is accompanied by a loss of birefringence, which is restored

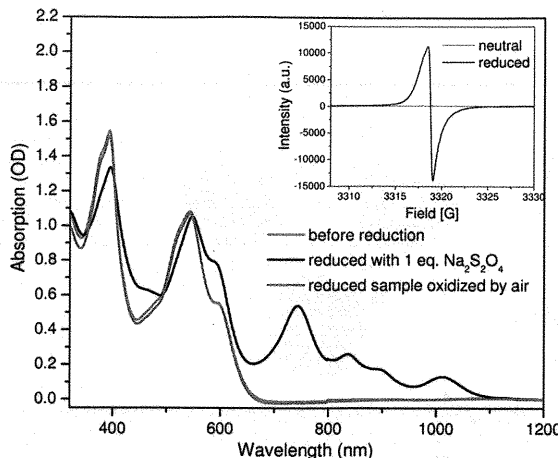


**Figure 11.** UV/vis spectra of aggregated solutions of **PP2b** ( $10^{-4}$  M) in water/THF mixture (80:20, v/v) before reduction (red), after reduction (black), and after exposing the reduced sample to air (blue). Inset: EPR spectrum of neutral (red) and reduced form (black).

after exposing the reduced fluid to air (Figure 10b). Thus, the structural change triggered by reversible charging causes the reversible switching of optical properties.

The reduced form shows a peak in the EPR spectrum, indicating paramagnetic species (Figure 11, inset), while the UV/vis spectrum of the reduced system shows four peaks in the near-infrared region, which represent a spectral signature of PDI radical anions (Figure 11).<sup>63–65</sup> Formation of the radical anions leads to the destruction of the gel network, most probably due to electrostatic repulsion and better solvation of the more polar anion species resulting in fission of the nanofibers. The UV/vis spectrum recorded after exposing the reduced sample to air is identical to that of the unreduced form, showing that reduced species are oxidized back to their neutral state by atmospheric oxygen (Figure 11). No evidence of decomposition is found after the reduction/oxidation cycle, indicating that the charging/discharging sequence is fully reversible.

The influence of reducing agent on the viscosity of **PP2b** at concentrations between  $10^{-5}$  M (dilute aggregated solution) and  $2 \times 10^{-2}$  M (gel) in water/THF (85:15, v/v) was investigated by rheological measurements (Figure 10c). Neutral samples exhibit shear thinning behavior (Figure 10c, inset), which is characteristic of linear polymers and wormlike aggregates that become aligned in the shear flow during the measurement.<sup>66</sup> In addition, samples with concentrations above the cgc show a yield stress, which is the finite stress required to achieve flow. The consistency coefficient  $K$  (measure of viscosity independent of shear rate) is obtained from fitting the shear rate vs shear stress plots to the standard Herschel–Bulkley model,  $\sigma = K\dot{\gamma}^n + \sigma_0$ , where  $\sigma$  is the shear stress,  $\dot{\gamma}$  is the shear rate,  $\sigma_0$  is the yield stress, and  $n$  is the flow behavior index.<sup>67</sup> In the presence of sodium dithionite,  $K$  drops drastically and the shear rate vs shear stress plot shows almost Newtonian behavior with no yield stress, even at high concentrations (Figures 10c (inset), S8). This dramatic drop in viscosity corroborates the destruction of the gel network. Oxidation results in restoration of the rheological behavior of the neutral systems, and the gel restores its initial elastic response (Figure S9).

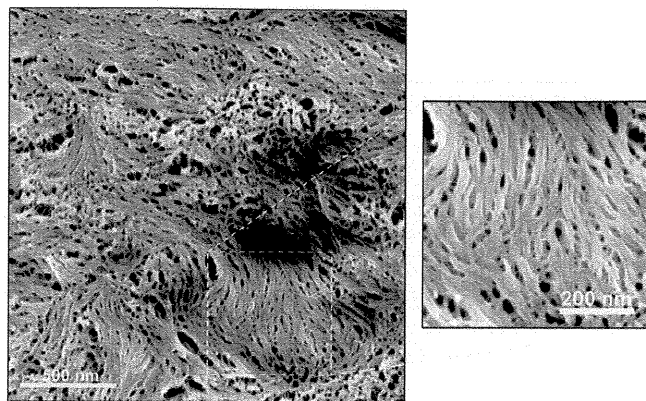


**Figure 12.** Cryo-SEM image of the thermally shrunken gel of **PP2b** ( $8 \times 10^{-3}$  M, water/THF mixture (80:20)).

The supramolecular structure of the gel after a reduction/oxidation cycle is indistinguishable from that observed prior to this cycle, as evidenced from cryo-SEM images (compare Figures 6 and S6). The restoration of the supramolecular structure is essential for the reversibility observed in the switching of rheological properties and birefringence.

The gel also shows a remarkable temperature-dependent behavior. Commonly, supramolecular gels exhibit a thermally reversible gel/sol phase transition at moderate temperatures because of the weak noncovalent interactions involved in gelation.<sup>5</sup> In contrast, the **PP2b** gel is stable toward change in temperature: it can be heated to 70 °C for at least 1 h without showing any change. Apparently, neither fiber fission occurs at this temperature nor the entanglement of the fibers is substantially weakened, which highlights the robustness of the noncovalent bonding responsible for the self-assembly of **PP2b**. Further heating to 100 °C does not lead to gel/sol phase transition. Instead, shrinkage of the gel is observed, leading to expulsion of a large fraction (~75 vol %) of the clear solvent mixture (Figures 13, S10). The shrinkage process is very rapid<sup>11</sup> (full shrinkage after only 90 s) and represents a rare example of the thermally triggered deswelling of a supramolecular gel.<sup>12</sup> Cryo-SEM of the shrunken gel reveals a very dense network of thick fiber bundles (Figure 12). Cavities between these bundles are much smaller than those in the swollen gel. The shrinkage is most probably due to a complex interplay between the hydrophobic effect and solvation of PEGs at higher temperatures.

The shrinkage is reversible in several ways. When slowly cooling the shrunken gel to room temperature, it expands spontaneously to its original volume. However, the swelling process is slow and completed only after ~24 h (Figure S10). The swollen gel form can be restored faster than that by sonication the sample for 1 h at ~40 °C.

The fastest way to restore the swollen gel is by exploiting the stimuli-responsiveness toward chemical reduction/oxidation. Addition of 1 equiv of aqueous sodium dithionite (at room temperature in the presence of air) to the solution surrounding the shrunken gel creates a temporarily fluid solution of reduced **PP2b**, followed by its gelation within several minutes due to oxidation by atmospheric oxygen (Figure 13). The temperature-triggered deswelling was repeated three times using sonication and another three times using reversible charging for restoration of the swollen gel, without any change in its responsiveness. Oscillatory rheological measurements show that the elastic response of the gel is fully restored after a shrinkage/swelling cycle (Figure S9). The switching between swollen gel, shrunken

(65) Gosztola, D.; Niemczyk, M. P.; Svec, W.; Lukas, A. S.; Wasielewski, M. R. *J. Phys. Chem. A* **2000**, *104*, 6545–6551.

(66) Dreiss, C. A. *Soft Matter* **2007**, *3*, 956–970.

(67) Steffe, J. F. *Rheological Methods in Food Process Engineering*; Freeman Press: 1996.

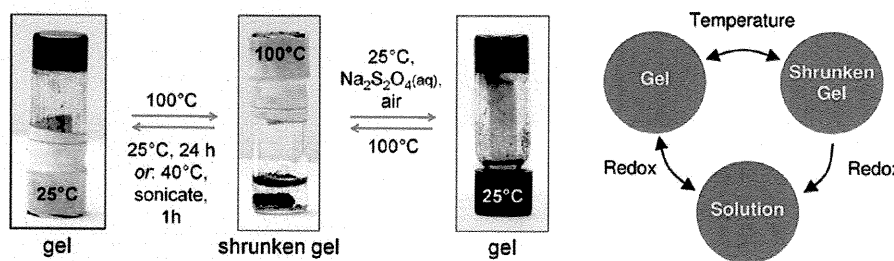


**Figure 13.** Left: Shrinkage of the gel of **PP2b** ( $8 \times 10^{-3}$  M, water/THF (80:20, v/v)) in response to the rise in temperature. The completely swollen gel is obtained back after 24 h at room temperature. It can be obtained more rapidly by either sonicating at 40 °C for 1 h or by addition of 1 equiv of  $\text{Na}_2\text{S}_2\text{O}_4$ (aq) in the presence of air. Right: Reversible switching between swollen gel, shrunken gel, and solution by exploiting response to temperature and reversible charging.

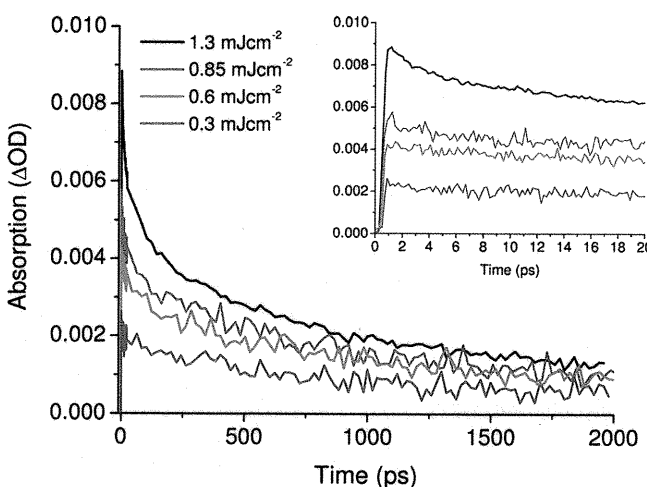


**Figure 14.** Decay kinetics of an aggregated **PP2b** ( $10^{-4}$  M) solution in water/THF (80:20, v/v) pumped at different energies and probed at the absorption peak (735 nm). The inset shows the first 20 ps of the transients.

gel, and fluid solution by exploiting dual responsiveness is depicted schematically in Figure 13. Such interconnected responsiveness allows great latitude in the design of functional adaptivity, which together with robustness may be useful for construction of self-assembled multiresponsive systems.

**Energy Transfer.** Relevant to light harvesting applications, **PP2b** assemblies strongly absorb visible light (Figure 8), while interactions between the chromophore units are expected to result in efficient excitation energy transfer. Femtosecond transient absorption studies on the disaggregated and aggregated **PP2b** (solution and gel state) reveal multiexponential decay of the excited state features. In the disaggregated state (chloroform solution, Figure S11, Table S1) the decays do not show power dependence, while the aggregated state (solution and gel) is characterized by power dependent kinetics (Figures 14, 15, S12, S13; Tables 1, 2). The power dependent decay in samples containing aggregated **PP2b** indicates that exciton annihilation takes place, which is typical of chromophore aggregates where a high photon flux of a laser pulse results in multiple excitations that bring about exciton annihilation processes. The complex power-dependent behavior may be attributed to various annihilation processes (delocalized and localized excitons, complex high-order multiexciton processes),<sup>68</sup> complicating the elucidation of energy transfer patterns.

Employing a widely used approximation, the site-to-site exciton hopping time constant,  $\tau_{\text{hop}}$ , can be estimated from the

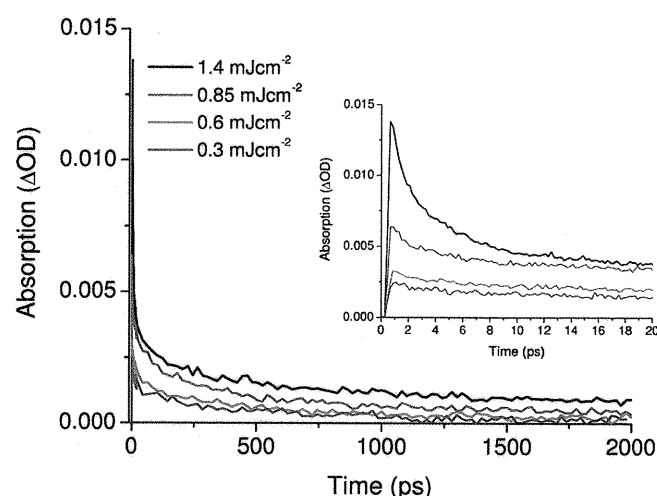


**Figure 15.** Decay kinetics of the gel sample of **PP2b** ( $8 \times 10^{-3}$  M) in water/THF (80:20, v/v) pumped at different energies and probed at the absorption peak (725 nm). The inset shows the first 20 ps of the transients.

**Table 1.** Time Constants and Their Amplitudes (In Parentheses) Contributing to the Decay Kinetics of the Transient Absorption Spectrum (See Supporting Information) of an Aggregated Solution of **PP2b** ( $10^{-4}$  M) in Water/THF (80:20, v/v), Excited with Different Pump Fluences<sup>a</sup>

pump fluence <b>PP2b</b> molecules per photon	$1.3 \text{ mJ cm}^{-2}$	$0.85 \text{ mJ cm}^{-2}$	$0.6 \text{ mJ cm}^{-2}$	$0.3 \text{ mJ cm}^{-2}$
$\tau_1/\text{ps}$	1.65 (0.20)	1.6 (0.18)	1.5 (0.12)	5.4 (0.12)
$\tau_1/\text{ps}$	1.65 (0.20)	1.6 (0.18)	1.5 (0.12)	5.4 (0.12)
$\tau_2/\text{ps}$	20 (0.23)	36 (0.17)	23 (0.13)	40 (0.10)
$\tau_2/\text{ps}$	261 (0.26)	400 (0.28)	280 (0.27)	560 (0.34)
$\tau_4/\text{ps}$	>2000 (0.31)	>2000 (0.36)	>2000 (0.48)	>2000 (0.43)

<sup>a</sup> The number of **PP2b** per photon (based on laser power; see Supporting Information) is also given.

annihilation time constant,  $\tau_{\text{an}}$  (corresponding to  $\tau_1$  and  $\tau_2$ ), using an “exciton random walk” model that has been shown to give satisfactory results for both natural and artificial chromophore aggregates.<sup>69,70</sup> According to this model  $\tau_{\text{an}} = (\pi^{-1}N \ln N + 0.2N - 0.12)\tau_{\text{hop}}$ , where  $N$  is the number of hopping sites. Using the kinetics components for the two fastest processes ( $\tau_1$  and  $\tau_2$ ) and the calculated number of hopping sites, we could estimate the corresponding hopping times of ~300 fs and ~4 ps for the gel, along with ~800 fs and ~12 ps for the solution.

(69) Montroll, E. W. *J. Math. Phys.* **1969**, *10*, 753–765.

(70) Ahrens, M. J.; Sinks, L. E.; Rybtchinski, B.; Liu, W.; Jones, B. A.; Giaimo, J. M.; Gusev, A. V.; Goshe, A. J.; Tiede, D. M.; Wasielewski, M. R. *J. Am. Chem. Soc.* **2004**, *126*, 8284–8294.

**Table 2.** Time Constants and Their Amplitudes (in Parentheses) Contributing to the Decay Kinetics of the Transient Absorption Spectrum of the Gel of **PP2b** ( $8 \times 10^{-3}$  M) in Water/THF (80:20, v/v), Excited with Different Pump Fluences (See Supporting Information)<sup>a</sup>

pump fluence <b>PP2b</b> molecules per photon	1.4 mJ cm <sup>-2</sup>	0.85 mJ cm <sup>-2</sup>	0.6 mJ cm <sup>-2</sup>	0.3 mJ cm <sup>-2</sup>
	3.7	6.2	9.4	18.7
$\tau_1/\text{ps}$	0.6 (0.45)	1.7 (0.38)	2 (0.27)	2.3 (0.29)
$\tau_2/\text{ps}$	5 (0.31)	29 (0.23)	26 (0.23)	45 (0.23)
$\tau_3/\text{ps}$	130 (0.15)	290 (0.25)	250 (0.32)	435 (0.32)
$\tau_4/\text{ps}$	>2000 (0.09)	>2000 (0.14)	>2000 (0.18)	>2000 (0.16)

<sup>a</sup> The number of **PP2b** per photon (based on laser power, see Supporting Information) is also given.

By using a similar model derived for a three-dimensional cubic lattice,<sup>69</sup> we obtained hopping times of ~150 fs and ~2 ps for the gel as well as ~300 fs and 4 ps for the solution. For comparison, the hopping time constants observed for various self-assembled PDI aggregates are similar (and analogous to the ones observed in natural light harvesting systems) to those we observe for **PP2b** assemblies: in aqueous solutions  $\tau_{\text{hop}} = 220\text{--}900$  fs and 4–18 ps,<sup>57</sup> while in organic medium  $\tau_{\text{hop}} = 5$  ps.<sup>70</sup> It should be noted that the estimation of hopping times is limited by the approximate character of the models. To distinguish between different possible modes of exciton delocalization in the complex hierarchical structures, development of models taking into account specific structural features of the systems will be needed.

Gels capable of excitation energy transfer have been suggested as promising systems for light harvesting.<sup>1,9,42,49,50,71</sup> The good exciton mobility, excellent light absorption properties, and stability toward heat and light suggest that the gel based on **PP2b** represents an advantageous light harvesting scaffold. Whereas several organogels based on PDI derivatives have been developed and suggested for application as light harvesting structures, sensors, and photonic devices,<sup>46–48,72,73</sup> the system presented herein is based on hydrophobic interactions, having

(71) Ajayaghosh, A.; Praveen, V. K. *Acc. Chem. Res.* **2007**, *40*, 644–656.

(72) Li, X.-Q.; Stepanenko, V.; Chen, Z.; Prins, P.; Siebbeles, L. D. A.; Würthner, F. *Chem. Commun.* **2006**, 3871–3873.

(73) Seki, T.; Yagai, S.; Karatsu, T.; Kitamura, A. *Chem. Lett.* **2008**, *37*, 764–765.

many characteristics of *hydrogels*. To the best of our knowledge, PDI-based hydrogels have not been reported.

In conclusion, we have demonstrated that in aqueous media **PP2b** self-assembles into extended supramolecular fibers that form a robust three-dimensional network structure resulting in gelation. This supramolecular gel shows robustness and multiple stimuli-responsiveness. Reversible charging of **PP2b** allows for switching between the gel state and fluid solution. Simultaneously, this provides a method for switching on and off the material's birefringence. Temperature triggered shrinkage of the gel leads to the (reversible) expulsion of a large fraction of the aqueous solvent. The dual sensibility toward chemical reduction and temperature with distinct and interrelated response to each of these stimuli allows for adaptive behavior and convenient property switching. In addition to stimuli-responsiveness, excellent light absorption and exciton mobility characteristics of the gel render it valuable as a scaffold for light harvesting applications.

**Acknowledgment.** This work was supported by grants from the Israel Science Foundation (Grant No. 917/06) and the Helen and Martin Kimmel Center for Molecular Design. The cryo-EM studies were conducted at the Irving and Cherna Moskowitz Center for Nano and Bio-Nano Imaging (Weizmann Institute). Transient absorption studies were performed at the Dr. J. Trachtenberg laboratory for photobiology and photobiotechnology (Weizmann Institute) and were supported by a grant from Ms. S. Zuckerman (Toronto, Canada). B.R. holds the Abraham and Jennie Fialkow Career Development Chair. We thank Prof. Samuel Safran for valuable discussions; Dr. Lev Weiner for EPR measurements; Dr. Nir Kampf, Jehonatan Shachaf, and Ehud Yarom for assistance with rheological measurements; the group of Prof. Lia Addadi for access to the optical microscope; and the groups of Profs. Jacob Klein, Victor Steinberg, and Dror Seliktar for access to their rheometers.

**Supporting Information Available:** Experimental details of synthesis and characterization of **PP2b**, additional electron microscopy images. This material is available free of charge via the Internet at <http://pubs.acs.org>.

JA903938G

**Table 2.** Time Constants and Their Amplitudes (in Parentheses) Contributing to the Decay Kinetics of the Transient Absorption Spectrum of the Gel of **PP2b** ( $8 \times 10^{-3}$  M) in Water/THF (80:20, v/v), Excited with Different Pump Fluences (See Supporting Information)<sup>a</sup>

pump fluence <b>PP2b</b> molecules per photon	1.4 mJ cm <sup>-2</sup>	0.85 mJ cm <sup>-2</sup>	0.6 mJ cm <sup>-2</sup>	0.3 mJ cm <sup>-2</sup>
	3.7	6.2	9.4	18.7
$\tau_1/\text{ps}$	0.6 (0.45)	1.7 (0.38)	2 (0.27)	2.3 (0.29)
$\tau_2/\text{ps}$	5 (0.31)	29 (0.23)	26 (0.23)	45 (0.23)
$\tau_3/\text{ps}$	130 (0.15)	290 (0.25)	250 (0.32)	435 (0.32)
$\tau_4/\text{ps}$	>2000 (0.09)	>2000 (0.14)	>2000 (0.18)	>2000 (0.16)

<sup>a</sup> The number of **PP2b** per photon (based on laser power, see Supporting Information) is also given.

By using a similar model derived for a three-dimensional cubic lattice,<sup>69</sup> we obtained hopping times of ~150 fs and ~2 ps for the gel as well as ~300 fs and 4 ps for the solution. For comparison, the hopping time constants observed for various self-assembled PDI aggregates are similar (and analogous to the ones observed in natural light harvesting systems) to those we observe for **PP2b** assemblies: in aqueous solutions  $\tau_{\text{hop}} = 220\text{--}900$  fs and 4–18 ps,<sup>57</sup> while in organic medium  $\tau_{\text{hop}} = 5$  ps.<sup>70</sup> It should be noted that the estimation of hopping times is limited by the approximate character of the models. To distinguish between different possible modes of exciton delocalization in the complex hierarchical structures, development of models taking into account specific structural features of the systems will be needed.

Gels capable of excitation energy transfer have been suggested as promising systems for light harvesting.<sup>1,9,42,49,50,71</sup> The good exciton mobility, excellent light absorption properties, and stability toward heat and light suggest that the gel based on **PP2b** represents an advantageous light harvesting scaffold. Whereas several organogels based on PDI derivatives have been developed and suggested for application as light harvesting structures, sensors, and photonic devices,<sup>46–48,72,73</sup> the system presented herein is based on hydrophobic interactions, having

- (71) Ajayaghosh, A.; Praveen, V. K. *Acc. Chem. Res.* **2007**, *40*, 644–656.
- (72) Li, X.-Q.; Stepanenko, V.; Chen, Z.; Prins, P.; Siebbeles, L. D. A.; Würthner, F. *Chem. Commun.* **2006**, 3871–3873.
- (73) Seki, T.; Yagai, S.; Karatsu, T.; Kitamura, A. *Chem. Lett.* **2008**, *37*, 764–765.

many characteristics of hydrogels. To the best of our knowledge, PDI-based hydrogels have not been reported.

In conclusion, we have demonstrated that in aqueous media **PP2b** self-assembles into extended supramolecular fibers that form a robust three-dimensional network structure resulting in gelation. This supramolecular gel shows robustness and multiple stimuli-responsiveness. Reversible charging of **PP2b** allows for switching between the gel state and fluid solution. Simultaneously, this provides a method for switching on and off the material's birefringence. Temperature triggered shrinkage of the gel leads to the (reversible) expulsion of a large fraction of the aqueous solvent. The dual sensibility toward chemical reduction and temperature with distinct and interrelated response to each of these stimuli allows for adaptive behavior and convenient property switching. In addition to stimuli-responsiveness, excellent light absorption and exciton mobility characteristics of the gel render it valuable as a scaffold for light harvesting applications.

**Acknowledgment.** This work was supported by grants from the Israel Science Foundation (Grant No. 917/06) and the Helen and Martin Kimmel Center for Molecular Design. The cryo-EM studies were conducted at the Irving and Cherna Moskowitz Center for Nano and Bio-Nano Imaging (Weizmann Institute). Transient absorption studies were performed at the Dr. J. Trachtenberg laboratory for photobiology and photobiotechnology (Weizmann Institute) and were supported by a grant from Ms. S. Zuckerman (Toronto, Canada). B.R. holds the Abraham and Jennie Fialkow Career Development Chair. We thank Prof. Samuel Safran for valuable discussions; Dr. Lev Weiner for EPR measurements; Dr. Nir Kampf, Jehonatan Shachaf, and Ehud Yarom for assistance with rheological measurements; the group of Prof. Lia Addadi for access to the optical microscope; and the groups of Profs. Jacob Klein, Victor Steinberg, and Dror Seliktar for access to their rheometers.

**Supporting Information Available:** Experimental details of synthesis and characterization of **PP2b**, additional electron microscopy images. This material is available free of charge via the Internet at <http://pubs.acs.org>.

JA903938G

Ex-5

98/100

- 1) Because of spin-statistics, electron-hole recombination leads to 25% singlet and 75% triplet state population. In organic molecules, only the singlets fluoresce, while the triplet excitation energy is transferred into heat. In organometallic compounds (of transition metals) due to spin-orbit coupling of the excited state to the metal orbitals there is a very efficient intersystem crossing to the lowest energy triplet state. That is triplet harvesting: singlet states are harvested into triplet states by S.O.C. In principle, a triplet emitter can exhibit a four times higher electroluminescence efficiency than a singlet emitter.
- 2) a. In the first stage of the photosynthesis process light is being absorbed by the chromospheres on the different photosystems. The chromospheres are excited to a higher electronic level. Then due to the energy gap cascade (the absorption wavelengths of the different chromospheres) there is a continuous energy transfer process from the B800 to the B850 in the LH II through the Forester ET mechanism, followed by energy transfer from LH II antenna systems to the LH I chromospheres, and from there to the reaction center. In the reaction center the excited P870 undergoes charge separation, and a stepwise electron transfer through the different components of the reaction center coupled to a proton transfer. The hole is transferred to P960 and turns it into  $P960^+$ . The electron is transferred to a quinone-A and at the same time a hole is transferred from the  $P960^+$  to a cytochrome subunit above the reaction centre. The electron is transferred to quinone-B which is mobile (not bound to the protein). Two electrons are required to fully reduce  $Q_B$  to  $QH_2$  taking up two protons from the cytoplasm in the process. The reduced quinone  $Q_BH_2$  diffuses through the membrane to another protein complex where its reducing power is used to reduce water and to create a proton gradient. The proton gradient is used by ATPase complex to produce ATP and from that energy rich hydrocarbons.
- b. The main reason for the directionality of the process is that after the photoinduced charge separation, the electron and hole transfer from the P870 in opposite directions in very quick reactions, in order to avoid the recombination process. The reaction center is set to accommodate this reaction by the positions of the  $BChl$  to accept the electron and the cytochrome to accept the hole. Moreover due to the protein polarity enhancement one electron oxidation is more significantly biased to the "left-side".

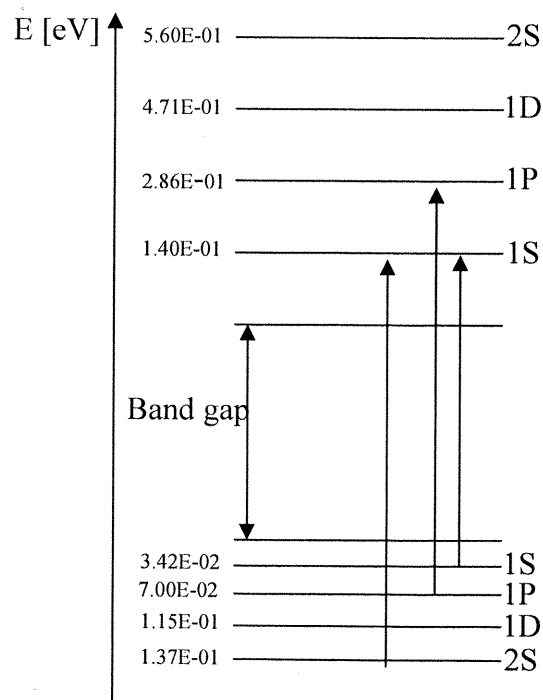
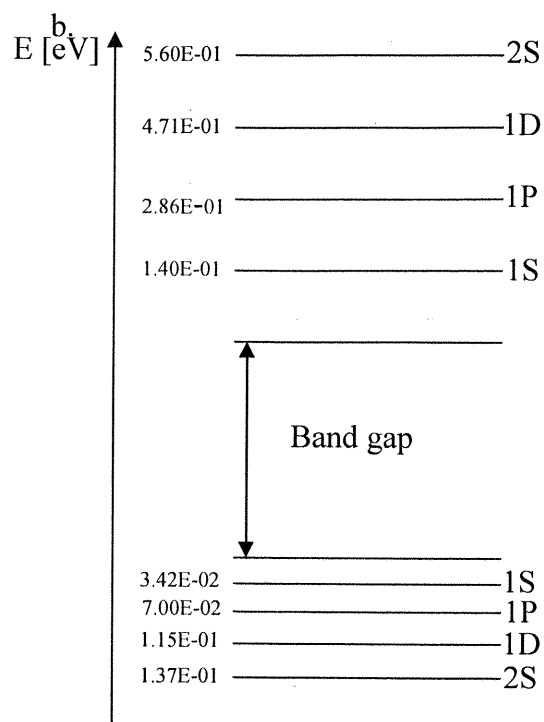
*canceled*

- 3) a.

The energies of the first 4 excited states are:

E [J]	1s	1p	1d	2s
$e^-$	2.24E-20	4.58E-20	7.54E-20	8.96E-20
$h^+$	5.48E-21	1.12E-20	1.84E-20	2.19E-20

E [eV]	1s	1p	1d	2s
$e$	1.40E-01	2.86E-01	4.71E-01	5.60E-01
$h$	3.42E-02	7.00E-02	1.15E-01	1.37E-01



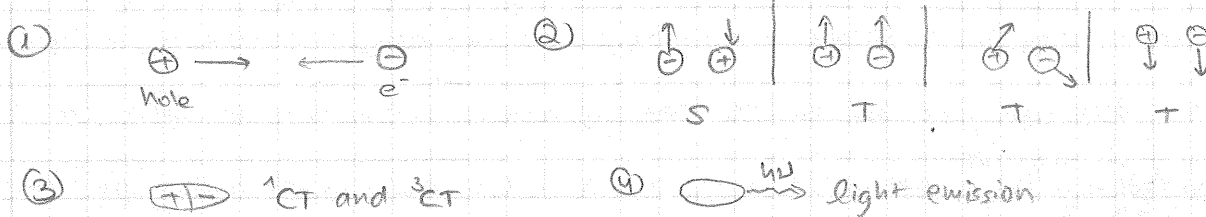
2) According to this roles the lowest energy transitions are:

- I)  $1S^h \text{ to } 1S^e - 1.74 + 0.14 + 0.034 = \underline{1.914 \text{ eV}}$
- II)  $2S^h \text{ to } 1S^e - 1.74 + 0.137 + 0.14 = \underline{2.017 \text{ eV}}$
- III)  $1P^h \text{ to } 1P^e - 1.74 + 0.286 + 0.07 = \underline{2.096 \text{ eV}}$

H1 Readability

94ffw

- ① In OLED, the population of excited states takes place via recombination of opposite charge carriers. This process forms excitons - which can be with different spin combinations - according to spin-statistics,  $e^-$ -hole recombination leads to  $2S^1$ - singlet and  $3S^1$ - triplet state population.



The exciton formation leads to relaxation by 4 singlet and 3 triplet paths and results in a populated lowest-excited singlet and triplet states.

Organic molecules can lead to fast decaying singlet emission  $S_1 \rightarrow S_0$  with high QY and  $\tau \sim ns$ , but the probability for a radiative  $T_1 \rightarrow S_0$  is very small and as a result of that 95% of the excitons are lost for the emission - their energy is transferred into heat. This problem can be solved by using organometallic complexes. The central metal ion induces spin-orbit coupling and results in a very efficient ISC to the lowest  $T_1$  state. The radiative transition  $T_1 \rightarrow S_0$  rate become larger for compounds with central metal ions with large SOC constants and the phosphorescence is more efficient (Calmet et al., 1997). In this way all 4 spin possibilities can be harvested to populate the lowest  $T_1$  - triplet harvesting - which may allow 4 times higher electro-luminescence efficiency than a singlet emitter.

- ② a. The system composed by non-covalent assembly of identical chromophores at specific distances and orientations. Light is absorbed by the chromophores on the different photosystems, and excited to a higher electronic level. Due to an energy gap cascade there is a continuous energy transfer process from  $B800 \rightarrow B850$  in the LHII through Forster energy transfer mechanism, and then there is an energy transfer from LHII antenna to LH1 chromophores and to the RC. In the RC there is a charge separation and stepwise electron transfer through different components that are coupled with proton transfer.

b. In order to prevent charge recombination - waste of the high energy elect.

by transferring it to heat. There are few factors that one needs to prevent it,

And that is the reason that the flow of electrons in the system is circular.

3. In TA instrument, during a single pump-probe experiment a pump beam

is being transferred through a sapphire plate to give white light (all wavelengths),

and excites the measured sample. A second beam - probe, is sent through the sample

(with a delay  $\tau$  with respect to the pump pulse). This delay is created by an optical

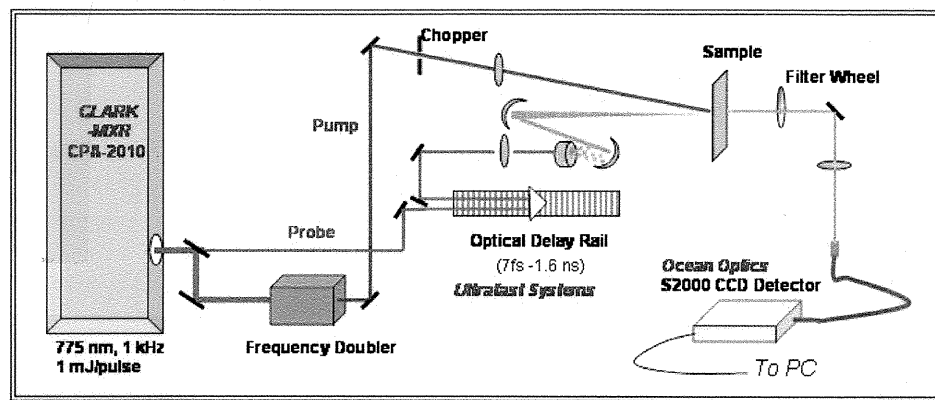
delay line which can be varied. From this measurement an absorption spectra can be

calculated - the excited sample minus the absorption of the sample in the ground state -  $\Delta A$ .

By changing the time of the delay ( $\tau$ ) between the pump and the probe and recording

the  $\Delta A$  spectrum at each time delay, a  $\Delta A$  profile as a function of  $\tau$  and the  $\lambda$

can be obtained.



4. a) Molecules A and B exhibit fluorescence despite the fact that two late

TMs are directly attached to the organic core since the electronic coupling is

relatively weak between Pd and the frontier T-orbitals of the PDT.

Very low

Therefore, there is no enhancement of spin-orbit coupling from the heavy atom as

could have been expected. (-1)

b) The short life times of these complexes's emission suggests emission from a singlet

state, and by TA studies a conformation for that was obtained.

The decay of  ${}^3\text{PDT}$  results in both fluorescence and intersystem crossing but in small

$g_T$  values. (6% for complex 1 and 20% for 2). the heavy atom effect

is relatively moderate in the T-bonded Pd-PDT complexes, because of the

poor overlap. The triplet state migrates to the PDT.

Because it is very low in energy it is not emissive! (-2)

c) In complex 3, according to the TA measurements, the decay is very fast which means that there is no fluorescence and that there is another competing mechanism that prevents the fluorescence of the complex. According to DFT calculations it was shown that this process is attributed to the ferrocen that serves as a good donor, but the excitation causes the PDI to promote an  $e^-$ , and the charge transfer resulted in a non-radiative fast decay.

5a) The UV-vis spectra shows a small red shift, broadening of the absorption bands and loss of absorption intensity that indicates ~~the~~ lower dipole interaction transition dipoles? (-3)

b) The fluorescence of the aggregate (in 20% THF or less) is quenched almost completely - indicating a high level of aggregation. what is left from the fluorescence shows a red shift which is characteristic of excimer fluorescence.

c) The exciton mobility was estimated from the annihilation time constant  $\tau_{\text{ann}}$  using the "exciton random walk" model. An estimation for the hopping times (of up to 300 fs and up to  $\tau_c$ ) for the aggregated material was obtained using this model. Another model for cubic lattice gave rise to hopping time of ~150 fs & 2 ps for the gel.

d) Gels that are capable of good excitation energy transfer are desirable for solar applications, since this system shows a good exciton mobility, high light absorption properties and great stability to heat and light it is classic for these kind of applications.

c) In complex 3, according to the TA measurements, the decay is very fast which means that there is no fluorescence and that there is another competing mechanisms that prevents the fluorescence of the complex. According to DFT calculations it was shown that this process is attributed to the ferrocen that serves as a good donor, but the excitation causes the PDT to promote an  $e^-$ , and the charge transfer resulted in a non-radiative fast decay.

Sa) The UV-VIS spectra shows a small red shift, broadening of the absorption bands and loss of absorption intensity that indicates ~~not~~ lower dipole interaction. transition dipoles? (-3)

b) The fluorescence of the aggregate (in 20% THF or less) is quenched almost completely - indicating a high level of aggregation. what is left from the fluorescence shows a red shift which is characteristic of excimer fluorescence.

c) The exciton mobility was estimated from the annihilation time constant  $\tau_{\text{ann}}$  using the "exciton random walk" model. An estimation for the hopping times of  $\sim 300 \text{ fs}$  and  $\sim 4 \text{ ps}$  ( $\tau_1, \tau_2$ ) for the aggregated material was obtained using this model. Another model for cubic lattice gave rise to hopping time of  $\sim 150 \text{ fs}$ ,  $\sim 2 \text{ ps}$  for the gel.

d) Gels that are capable of good excitation energy transfer are desirable for solar applications, since this system shows a good exciton mobility, high light absorption properties and great stability to heat and light. It is classic for these kind of applications.



1. What about the  
 shape of the  
 potential?   
 What will happen  
 with isotopes?

2. Nullikin said that as we  
 tend to lose the grasp of the chemical guiding  
 that will be justified →

3. We tend to have a level of understanding that will be justified →

4. Light shows

5. It means that for a heavy particle we  
 need for a larger gaps.

6. For lighter particles larger gaps.

7. Heavy atoms

8. Conc → would like to have a level of understanding that will be justified →

9. go

Yulia Tsverin

I.D. 319218665

## Molecular Photonics

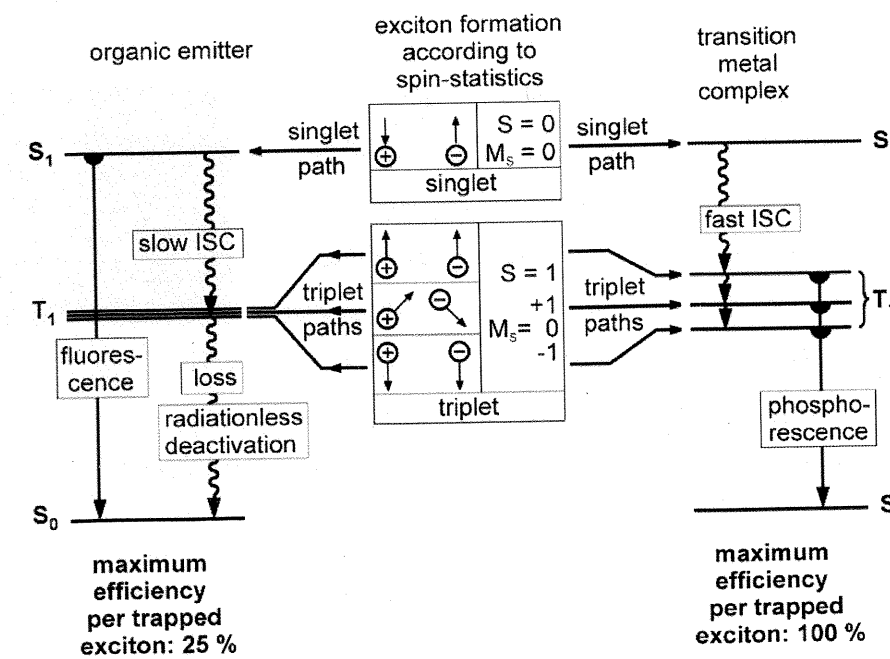
### Exercise 5

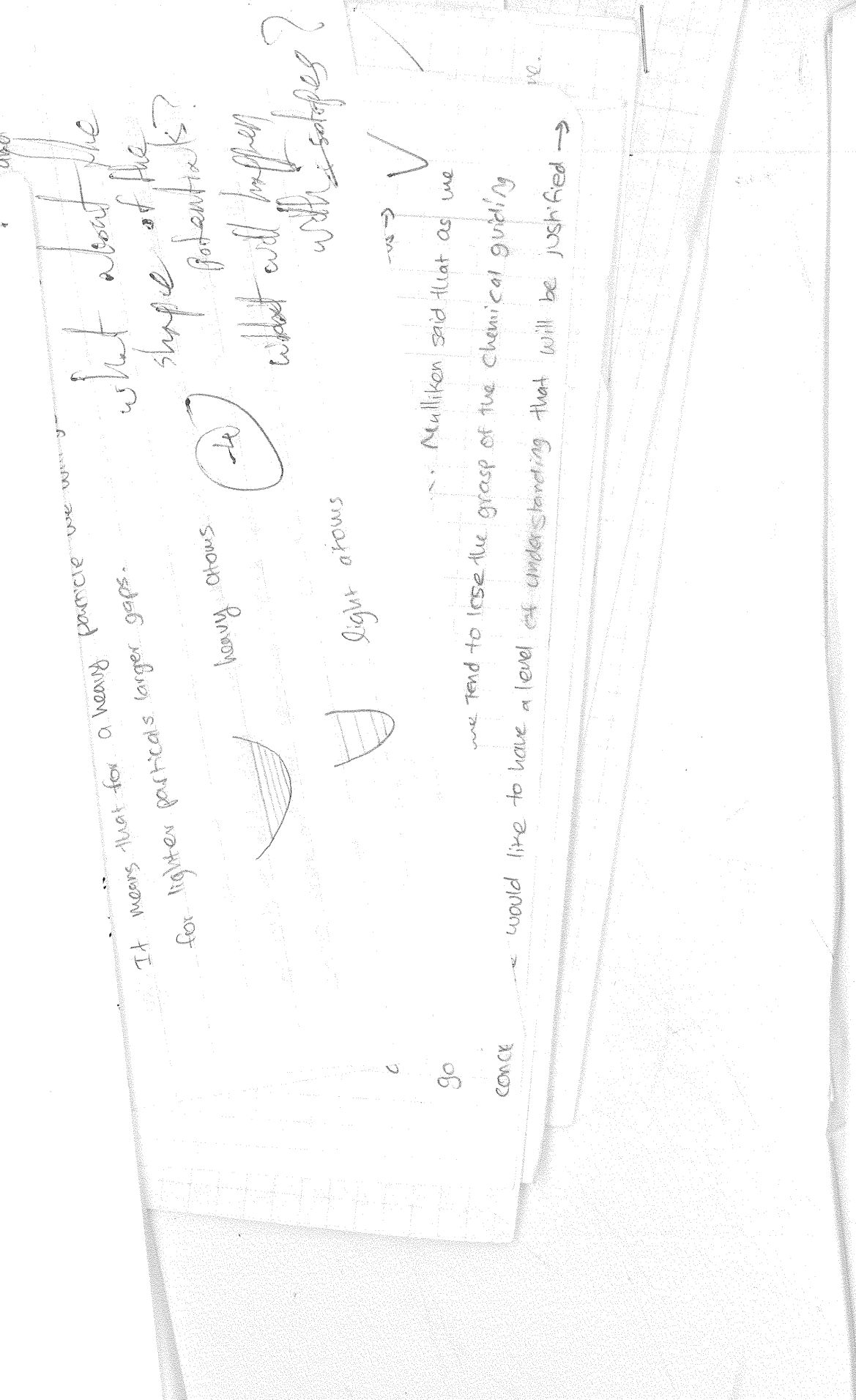
1.

In OLED the electro-luminescence process occurs due to recombination of negatively charged electrons and positively charged holes. The electron and hole are attracted to each other by coulomb forces and form excitons in the emission layer of an OLED. Due to spin combinations, electron-hole recombination leads to 25% singlet and 75% triplet state population. After the exciton is formed and the relaxations by one singlet and three triplet paths have occurred, the lowest excited singlet and triplet states are populated. This is valid for organic as well as for organo-transition-metal emitter materials.

In the case of organic molecules only the singlets emit light (fluorescence), while the triplet excitation energy is transferred into heat (left hand side of the picture below). But the organometallic compounds with transition metal centers have fast intersystemcrossing (ISC) to the lowest triplet state, due to significant spin-orbit coupling caused by central metal ion. The singlet emission is not exhibited in this process. In this case the triplet harvesting obtain a four times higher electro-luminescence efficiency with phosphorescent triplet emitters than with fluorescent singlet emitters (right hand side of the picture below).

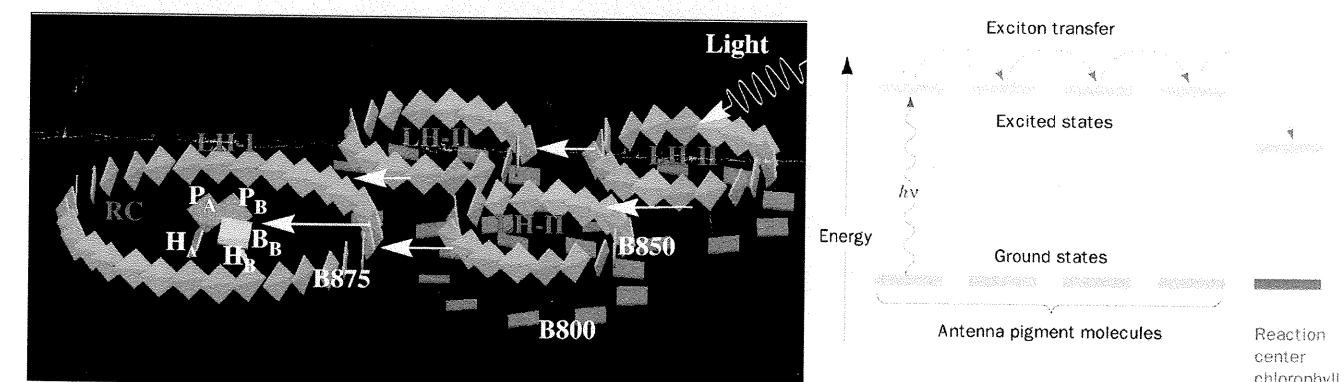
By choosing Organo-transition-metal compounds for OLED the more stable phosphorescence emission is achieved, leading for higher efficiency. Also, chemical stabilities obtainable with these compounds as compared to organic emitters.





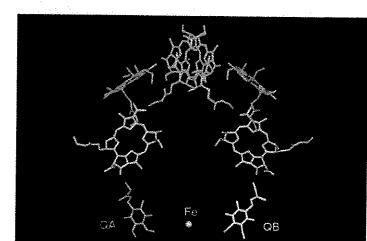
2.

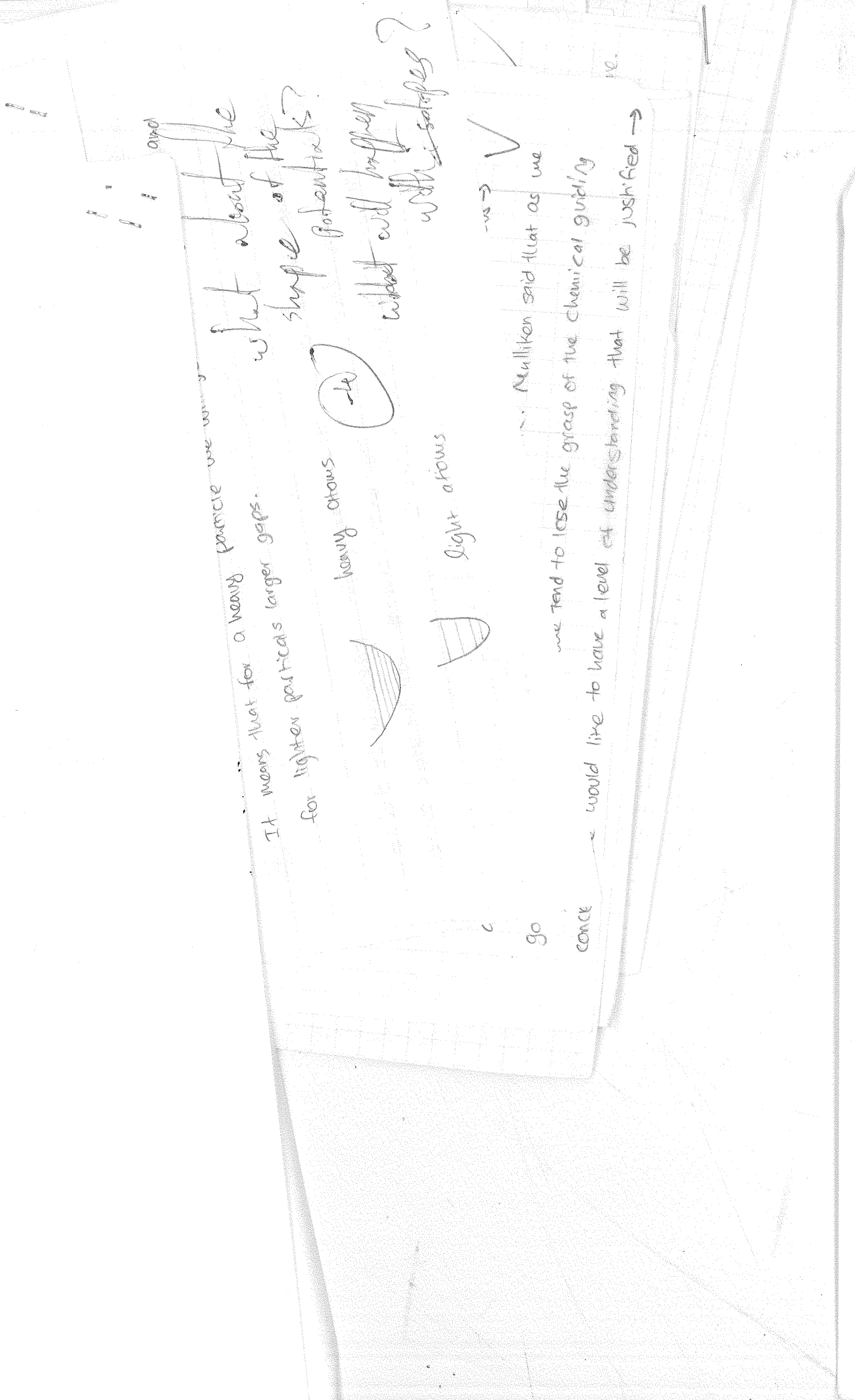
a. The photosynthetic system of purple bacteria consists of reaction center (RC, red) that are surrounded by the light-harvesting complex I (LH-I, green) to form the LH-I-RC complex, which is surrounded by multiple light-harvesting complexes LH-II (green), forming altogether the photosynthetic unit (PSU). In other words this complex consists of noncovalent assembly of identical chromophores at specific distance and orientations. This chromophores transfer the energy between them in the form of excitons through the gradient transition by the FRET mechanism. The light transition occurs as follows: B800-B850-B875 (antenna pigment molecules: B states for chlorophyll and 8XX states for the max. excitation wavelength) -P (reaction center chlorophyll).The excitation is trapped by the reaction center chlorophyll because its lowest excited state has a lower energy than those of the antenna pigment (chlorophyll) molecules.



b.

According to the given link  $Q_A$  is a tightly bounded molecule compared to a  $Q_B$  that is more loosely bounded and fairly easy to detach. Since the molecular structure seems to be symmetric the charge separation can occur in both directions. But in fact the charge separation is more likely to occur in  $Q_A$  rather in  $Q_B$ , probably due to kinetic reasons.  $Q_B$  bond is weaker because of when  $Q_B$  is reduced to  $QH_2$  it leaves the complex and diffuses through the membrane to another protein complex where it is oxidized. This behavior leads to not symmetrical flow of the electrons in the reaction center.





3.

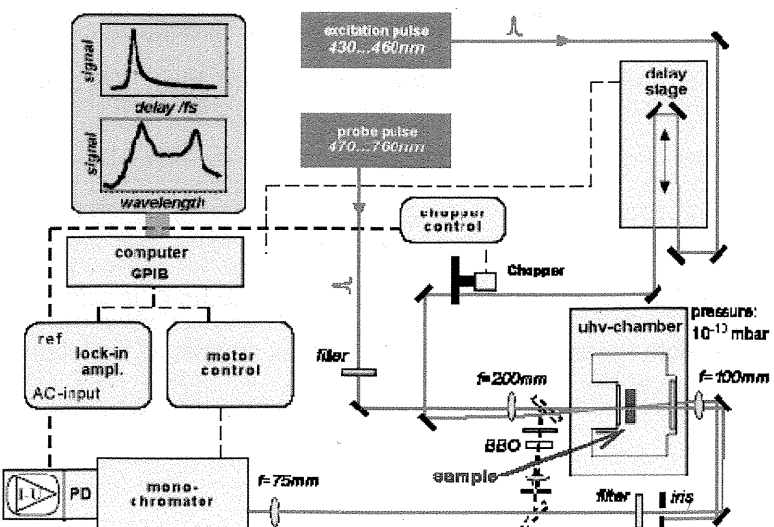
In the transient absorption instrument the light (laser pulses) is passed through a sample, separated to individual wavelengths by a monochromator, and measured with a detector. The light absorption of the sample can be detected from the decrease of the intensity. The measurement is referenced to the effect of the excitation pulse, while it measures the changes from a steady state in which the sample has not been excited – deviation from the steady state absorption are measured. The change is given by

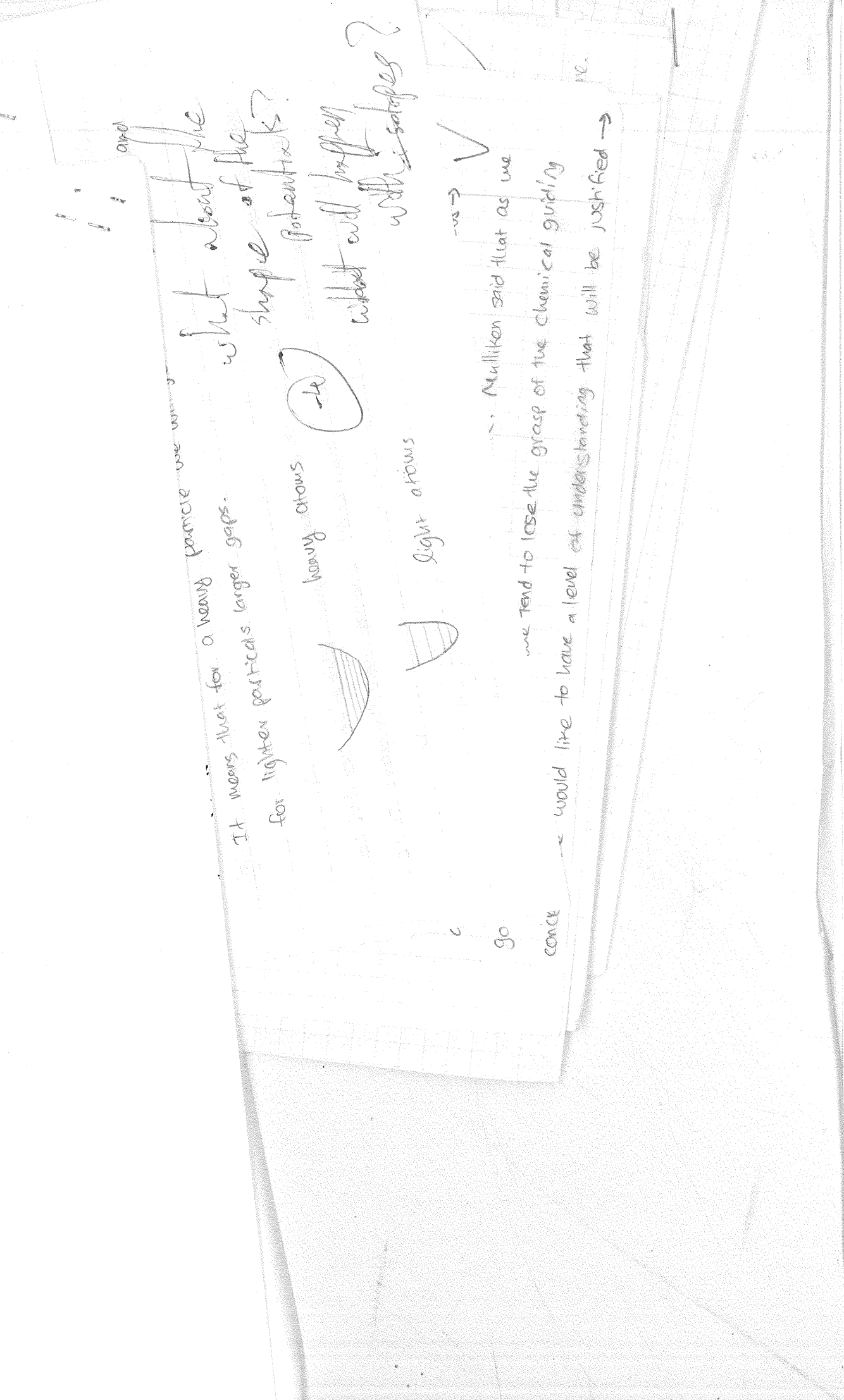
$$\Delta A = -\frac{\log(10)}{I}$$

Within the absorption spectrum of the excited state there will be a positive value to the measurement as excited molecules will absorb the light. Within the absorption spectrum of the ground state there will be a negative value to the measurement as there will be a depleted number of molecules in the ground state.

Since the electronics fail to measure phenomena shorter than picoseconds, the probe pulse is directed onto the sample with increasing delay time with respect to the pump pulse. Thus obtained cross correlation function contains information concerning the time dependent decay of the transient population and coherence generated by the pump pulse in the sample. The time delay stage is obtained by displacing the mirror that changes the path length of the light.

The information about the temporal evolution of the excited state which we are interested in, is collected by varying the temporal overlap between pump and probe pulse via the delay stage and measuring the time averaged transmission of the sample at each position of the delay. One ends up with a plot of time delay vs. absorption/transmission.





4.

- The molecules that are shown in the article are metal complexes based on perylene tetracarboxylic acid diimide (PDI) dyes, in which two palladium centers are attached to the dye aromatic core. These complexes show unexpectedly strong fluorescence despite the fact that two late transition metals are directly attached to an aromatic system of the organic dye. The heavy atom affect on spin orbital coupling by accelerating the spin flipping and “transferring” it to another orbit. The heavy atom increase the intersystem crossing that leads to the triplet state, the phosphorescence. So it was expected that these two complexes will exhibit high phosphorescence and low fluorescence. However, a heavy-atom effect is relatively moderate in Pd-PDI complexes, especially in the case of complex A, due to metal-carbon connecting through  $\sigma$ -bonds. As the result of this relatively weak electronic coupling between the metal-based orbitals and the dye  $\pi$  – system, the molecules exhibit high fluorescent. The TD-DFT calculations reveals that HOMO and LUMO, are both localized on the PDI ligand, with minor participation of the Pd centers in the frontier orbitals makeup. Thus, in complex A,  $\sigma$ -bonds connecting two late transition metal centers with the chromophore core do not bring about strong interaction between the Pd orbitals and PDI  $\pi$ -system, localizing the electronic excitation mostly on the PDI ligand. In the case of comlex B there is a stronger electronic coupling between PDI and Pd due to Pd dz<sub>2</sub> orbital participating in the HOMO makeup. But still it does not have strong influence on the intersystem crossing.
- As was described above the heavy atom effect expected to influence on the increasing rate of the intersystem crossing, leading to increase in the phosphorescence. But due to electronic structure of both complexes, the localization of the excitation electrons mostly on the PDI, the effect of the heavy atom is diminishing (decrease in the phosphorescence).
- From the femtosecond transient absorption spectroscopy graphs that are shown in the presentation, can be seen that the excitation life time the molecule C is very small (about  $\tau=1.67\text{ps}$ ) compared to others molecules. The complex C is consist of molecule ferrocene that acts as donor and due to excitation it suppose to create a charge separation of the

what about the shape of the potential?

( $\Delta$ )

heavy atoms

light atoms

go

conc

we tend to lose the grasp of the chemical guiding

that will be justified  $\rightarrow$

form  $D^+$  and  $A^-$ . But the PDI molecule during excitation produces an electron, due to its electronic structure, so it cannot act as an acceptor. This complex is complicated and an electron transfer should be studied. Probably molecule C does not show any emission because of all the energy is emitted as thermal energy.

5.

- The PP2b compound was found to form an aggregate in water solution due to hydrophobicity. And PP2b is disaggregated in various organic solvents, such as THF. The UV-vis spectrum of an aggregate showed broadening of the absorption bands, accompanied by some loss of absorption intensity, a slight red shift, and an inversion of relative intensities of 0-0 and 0-1 electronic transitions, typical of face-to-face stacking of PDI molecules. The interactions between the transition dipole are lowered.
- The aggregates are detected from the quenching in the fluorescence, while red-shifted fluorescence indicates on excimer fluorescence. From the studies it was found that PP2b assemblies strongly absorb visible light, and interactions between the chromophore units are expected to result in efficient excitation energy transfer. The femtosecond transient absorption studies on the aggregates showed multiexponential decay of the excited state features. The aggregated state is characterized by power dependent kinetics, while the dependent decay in aggregates indicates that exciton annihilation takes place. That is typical of chromophore aggregates where a high photon flux of a laser pulse results in multiple excitations that bring about exciton annihilation processes such as delocalized and localized excitons, complex high-order multiexciton processes. These processes complicate the elucidation of energy transfer patterns.
- From an "exciton random walk" model, the site-to-site exciton hopping time constant,  $\tau_{\text{hop}}$ , can be estimated from the annihilation time constant,  $\tau_{\text{an}}$ . According to this model  $\tau_{\text{an}} = (\pi - 1)N \ln N + 0.2N - 0.12\tau_{\text{hop}}$ , where  $N$  is the number of hopping sites. Using the kinetics components for the two fastest processes ( $\tau_1$  and  $\tau_2$ ) and the calculated number of hopping sites, the corresponding hopping times will be of ~300 fs and ~4 ps for the gel, along with ~800 fs and ~12 ps for the solution. By using a similar model derived for a

and  
what about the  
shape of the  
potentials?

to

heavy atoms



light atoms



go

conc

Malliken said that as we  
we tend to lose the grasp of the chemical bonding  
would like to have a level of understanding that will be justified →

ie.

three-dimensional cubic lattice, the obtained hopping times is ~150 fs and ~2 ps for the gel as well as ~300 fs and ~4 ps for the solution.

d. The gels that capable of excitation energy transfer can exhibit excellent light absorption properties, good exciton mobility, stability toward heat and light. Due to these properties the gels can be considered to use for light harvesting like solar energy conversion. In the article PP2b represents an advantageous light harvesting scaffold, due to its excellent light absorption and exciton mobility characteristics.